NMR Study of Calmodulin's Interaction with Inducible Nitric Oxide Synthase

by

Yay Duangkham

A thesis

presented to University of Waterloo

in fulfillment of the

thesis requirement for the degree of

Master of Science

in

Chemistry

Waterloo, Ontario, Canada, 2010

Author's Declaration

I hereby declare that I am the sole author of this thesis. This is a true copy of the thesis, including any required final revisions, as accepted by my examiners.

I understand that my thesis may be made electronically available to the public.

Yay Duangkham

Abstract

The increase of calcium in the cell can induce cellular functions such as fertilization, cell division and cell communication. Calcium (Ca^{2+}) carries out these processes through proteins called calcium sensors. An important calcium modulator is calmodulin. Calmodulin has four possible Ca^{2+} binding sites that have the characteristic helix-loop-helix (EF hand) motif. When the EF hands bind to Ca^{2+}, methionine rich hydrophobic patches are exposed allowing for CaM to interact with target proteins. However, there are proteins that can interact with CaM at low levels of Ca^{2+} or in the absence of Ca^{2+}.

An enzyme that is activated by CaM is nitric oxide synthase (NOS), which converts L-arginine to L-citrulline and nitric oxide (•NO), where •NO is used to carry out important cellular functions. There are three isoforms of the enzyme; endothelial, neuronal and inducible NOS. The first two isoforms are activated by Ca^{2+}-bound CaM when there is an influx of Ca^{2+} and are therefore Ca^{2+}-dependent whereas inducible NOS (iNOS) is activated and binds tightly to CaM regardless of the Ca^{2+} concentration and is therefore Ca^{2+}-independent. Of particular interest is the iNOS enzyme, since no three-dimensional structures of the reductase domain or the CaM-binding region have been solved.

All three isoforms of NOS exist as homodimers, where each monomer consisting of a reductase domain and an oxygenase domain separated by a CaM-binding region. The reductase domain contains binding sites for NADPH and the flavins, FAD and FMN, which facilitate electron transfer from the NADPH to the catalytic heme in the oxygenase domain of the opposite monomer. The transfer of electrons from the FAD to the heme is carried out by the FMN domain which is proposed to swing between the two docking points since the distance between the two points is too large for electron transfer. This electron transfer point is under the control of CaM,

which is essential for NOS activation. This dynamic process and the direct role of CaM have yet to be observed structurally. A method to monitor dynamics structurally is through the use of nuclear magnetic resonance (NMR) spectroscopy.

Therefore as the first step to determine the NMR structure of the FMN domain with the CaM-binding region, the structure of the iNOS CaM-binding region bound to CaM will be determined. The structure will allow for further characterization and identification of important interactions between the iNOS CaM-binding region and CaM which contribute to the unique properties of iNOS.

Acknowledgments

I would like to thank my supervisors Guy Guillemette and Thorsten Dieckmann for giving me their support, guidance and patience through my studies. The opportunity to work with such knowledgeable and kind supervisors was a pleasure.

Great thanks also go to my committee members, Michael Palmer and Elizabeth Meiering, for reading and reviewing my thesis and providing their input in my studies.

I would also like to thank my lab mates: Don Spratt, Odi Israel, Erika Murray, Valentina Taiakina, Genevieve Labbe, Clearance Wang, Malcolm Robb and Amanda Harrop for their friendship and support. A special appreciation goes to Don Spratt, who helped ease me into the lab and the project.

A special thanks also goes to Carolyn Steele for proofreading my thesis.

And lastly, my family members and Ian Lippert, who provided support outside of the lab.

Dedication

To the Duangkham family

and Ian Lippert

Table of Contents

List of Figures

List of Tables

List of Abbreviations

Å	Angstrom
AI	Autoinhibitory
BMRB	Biological Magnetic Resonance Bank
Ca^{2+}	Calcium
CaM	Calmodulin
CaM-iNOS peptide	CaM in complex with iNOS CaM-binding region
CARA	Computer Aided Resonance Assignment
CBD	Chitin-binding domain
CBD-intein-iNOS peptide	CaM-binding region attached to the fusion tag, intein with the chitin binding domain of iNOS
cNOS	Constitutive nitric oxide synthase
Da	Daltons (g/mol)
eNOS	Endothelial nitric oxide synthase
FAD	Flavin adenine dinucleotide
FMN	Flavin mononucleotide
FRET	Fluorescence resonance energy transfer
H_4B	Tetrahydrobiopterin
HSQC	Heteronuclear spin quantum correlation
IMPACT	Intein Mediated Purification with an Affinity Chitin-binding Tag
iNOS	Inducible nitric oxide synthase
iNOS peptide	iNOS peptide of the CaM-binding region
LB	Luria-Bertani broth
NADPH	Nicotinamide adenine dinucleotide phosphate
NOHA	N-Hydroxy-L-arginine
NMR	Nuclear magnetic resonance
nNOS	Neuronal nitric oxide synthase
NOESY	Nuclear overhauser effect spectroscopy
NOS	Nitric Oxide Synthase
PDB	Protein Data Bank
TOCSY	Total correlation spectroscopy

Chapter 1 Introduction

1.1 Calmodulin (CaM)

Calcium ions (Ca^{2+}) are present in all cellular systems and are the most abundant mineral in the body where 99% of the total concentration is present in the bone and the other 1% is located in the bodily fluids and in cells (Duyff, 2006). Calcium in cells acts as a secondary messenger by controlling some of the most important biological functions, which include fertilization, cell proliferation including division, cell communication, neuron transmission and cell death (Duyff, 2006). These functions are regulated by a family of Ca^{2+}-binding proteins that respond to changing intracellular Ca^{2+} concentrations. These Ca^{2+}-modulated proteins contain an EF hand motif which consists of a helix-loop-helix pattern where the calcium binds in the loop region (Figure 1.1). One of the most important proteins belonging to this family is calmodulin.
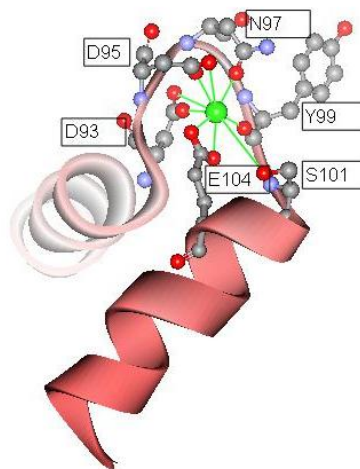
Figure 1.1. Ribbon structure of the EF hand motif with Ca^{2+} binding amino acids
The helix-loop-helix of the EF hand motif taken from the crystal structure of the third EF hand of CaM bound to Ca^{2+}. The amino acids represented by the ball and stick figures contribute to the binding of Ca^{2+} ion (green sphere) through negatively charged oxygen (red sphere attached to green line). The distributions of Ca^{2+} coordinating amino acids have the 1-3-5-7-9-12 position pattern. Made from PDB 1CLL using Accelrys DS visualize v2.5.1.

Calmodulin (CaM) is an essential protein because it is able to respond to changing intracellular Ca^{2+} concentrations and the target proteins it activates are responsible for several vital cellular functions including cell division, apoptosis, blood pressure, fertilization, intracellular communication and cell differentiation (Frederick et al., 2006, Benaim and Villalobo, 2002). It is a highly conserved small protein that consists of 148 amino acids and has a molecular weight of 17 kDa. CaM is present in most, if not all, eukaryotic cells and through its four EF hands, it binds to Ca^{2+} and is able to bind over a hundred proteins.

1.1.1 Structure of CaM

CaM has two globular regions referred to as the N- and C-terminal lobes which are separated by a highly flexible central linker region. In each lobe, there are two solvent exposed EF hand motifs that cooperatively bind to free Ca^{2+}. The C-terminus EF hands bind to Ca^{2+} with a higher affinity than the N-terminus, allowing for different forms of Ca^{2+} saturated CaM. A nuclear magnetic resonance (NMR) structure of Ca^{2+}-free (apo) CaM (Figure 1.2a) indicates that the two lobes move independently of each other due to the flexible central linker region, consisting of residue 77 to 81; and that the N-terminal lobe is a more resolved structure and not as dynamic as the C-lobe (Zhang et al., 1995, Kuboniwa et al., 1995).

N-terminal domain

C-terminal domain

a   b   c   d
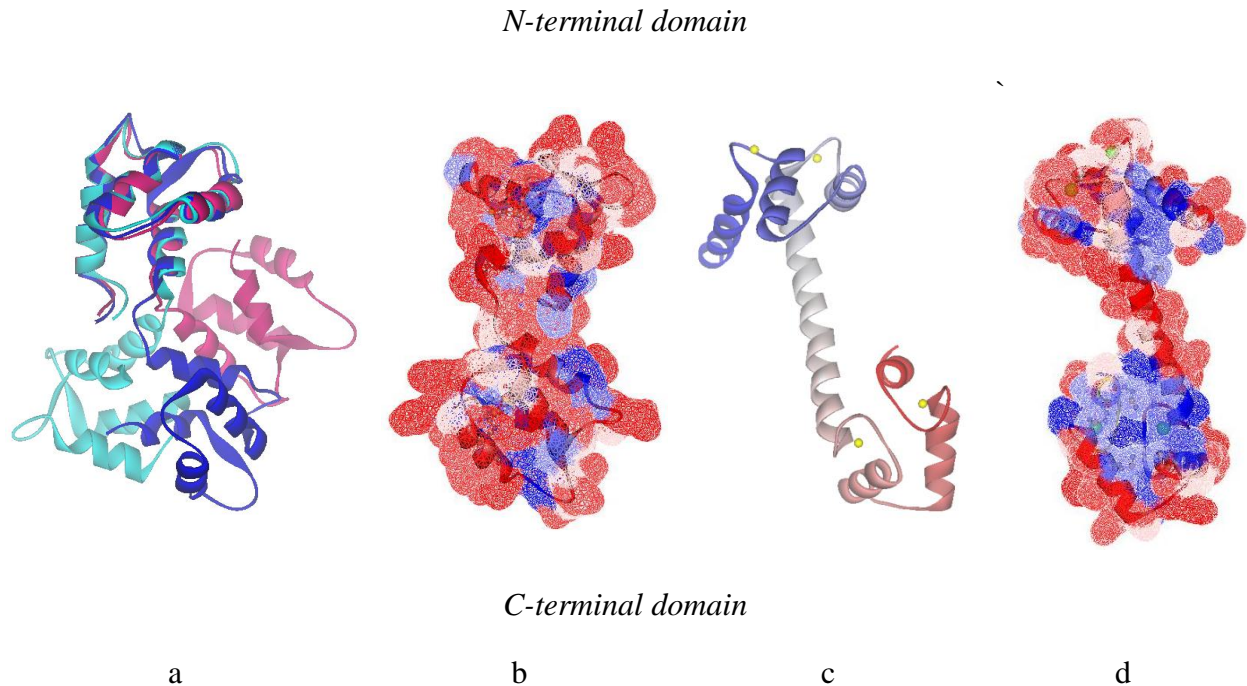
Figure 1.2. Structural comparison of CaM in its calcium free and bound forms
The structures of apo CaM and holo CaM in its ribbon structure and surface structure indicating hydrophobic patches are shown with the N-terminal domain as the top globular lobe and the C-terminal domain in the lower globular lobe. (a) Three possible conformations of thirty of the Ca^{2+}-free CaM determined by NMR spectroscopy show the N-terminal lobe remains in the same conformation whereas the C-terminal lobes are highly mobile. (b) The surface representation of hydrophobic patches (blue) of apo-CaM is mainly internalized compared to (d) that of the holo-CaM. (c) The crystal structure of Ca^{2+} (yellow spheres) saturated calmodulin with the central region elongated. Structures were made from PDB 1DMO and 1CLL for Ca^{2+}-free and bound respectively using Accelrys DS visualize 2.4.

When CaM binds Ca^{2+} (holo-CaM), the general secondary structure of the protein remains the same except that now the collapsed globular domains in the apo-CaM turn outwards to elongate the overall CaM structure to increase the distance between the domains (Babu et al., 1988, Kuboniwa et al., 1995, Zhang et al., 1995). During this conformational change, CaM exposes hydrophobic patches, which are larger in the C than the N-terminal lobe, (Figure 1.2d) allowing it to interact with its target proteins (Yamniuk and Vogel, 2004). The hydrophobic patches are enriched with nine methionines, four in each terminal domain and one in the centre linker region, which contribute 46% of the hydrophobic patches (Zhang et al., 1995). Relative to

other proteins, CaM has elevated levels of methionine which contributes to tight interaction with non-polar surfaces due to the thioether sulfur in the side chain to accommodate different non-polar binding surfaces (Gellman, 1991). The main mode of interaction is through hydrophobic interactions and van der Waals forces but electrostatic interactions are also important (Yamniuk and Vogel, 2004). In addition to the methionine rich hydrophobic patches, the central linker region also plays an important role by unraveling from the α-helix into random coil (O'Neil and DeGardo, 1990). The ability of the central linker to extend allows for the two terminal lobes to accommodate binding of different target proteins. Despite the crystal structure of the Ca^{2+}-CaM (Figure 1.2c) showing the centre linker as a rigid α-helix, NMR studies indicate the centre linker still remains very flexible and still allows for independent movement of the two domains (Barbato et al., 1992).

1.1.2 Ca^{2+}-dependent and Ca^{2+}-independent Calmodulin binding to Target Proteins

Calmodulin can bind to target proteins in a Ca^{2+}-dependent or Ca^{2+}-independent manner based on whether the target proteins can bind to holo-CaM during an increase of intracellular Ca^{2+} or to apo-CaM at basal Ca^{2+} levels.

Ca^{2+}-dependent target proteins require Ca^{2+} bound CaM which occurs when Ca^{2+} concentration is above the basal level. At resting Ca^{2+} levels the concentration of Ca^{2+} is 0.1 μM and can increase over one hundredfold to 10 μM (Roskoski, 1996, Van Eldik and Watterson, 1998). The sequence of CaM-binding regions of Ca^{2+}-dependent target protein varies, however they are typically 16-30 amino acids in length and are basic amphiphilic α-helical, containing bulky hydrophobic amino acids (Yamniuk and Vogel, 2004, O'Neil and DeGardo, 1990, Afshar et al., 1994). Hydrophobic amino acids are arranged three to four amino acids apart so they stack

on top of each other in the α-helix creating a parallel hydrophobic surface or, in some target proteins, a hydrophobic curved surface on the α-helix (O'Neil and DeGardo, 1990). The hydrophobic patches of CaM in the terminal lobes bind are shown to bind to bulky hydrophobic amino acids that are separated by 8 or 12 residues (Afshar et al., 1994). Typical bulky hydrophobic amino are the aromatic or long side chained nonpolar amino acids. The hydrophobic amino acids that bind to the hydrophobic patches of CaM are termed anchoring residues, these allow for other hydrophobic residues in between them to interact with CaM (Yamniuk and Vogel, 2004). Based on sequence alignment of Ca^{2+}-dependent CaM-binding regions, conserved positions of bulky hydrophobic residues are arranged in a 1-8-14, 1-5-8-14 or 1-5-10 motif; where the numbering system starts with the first hydrophobic residue and the two outer numbers represent the anchoring residues (Yamniuk and Vogel, 2004, Rhoads and Friedberg, 1997). Along with hydrophobic amino acids, target proteins also contain positively charged basic amino acids that give the CaM-binding regions their amphiphilic property. These basic residues are located on the opposite side of the hydrophobic patches in the α-helix and interact mainly with the central linker region of CaM, which is lined with negatively charged amino acid (O'Neil and DeGardo, 1990, Afshar et al., 1994). These residues account for the electrostatic interactions with CaM. There are variations in the binding motifs described above as well as target proteins that have a very different binding motif (Rhoads and Friedberg, 1997).

Target proteins that are categorized as Ca^{2+}-independent can bind to CaM in the absence of Ca^{2+} or at very low basal concentration of Ca^{2+}. Included in this group of proteins are those that bind only to apo-CaM, such as neuromodulin, that are thought to act as an intracellular CaM storage protein until Ca^{2+} concentration increases (Jurado et al., 1999). The majority of proteins classified as Ca^{2+}-independent are target proteins that bind tightly to CaM in the presence and

absence of CaM (Rhoads and Friedberg, 1997). A known sequence that binds to apo-CaM is the consensus IQ motif which has the general form IQXXXRGXXXR, where I, Q, R, G and X represent the amino acids isoleucine, glutamic acid, arginine, glycine and any amino acid respectively (Rhoads and Friedberg, 1997). The isoleucine can be replaced with a leucine or valine and the X amino acid may also play a role in the binding (Jurado et al., 1999). The IQXXX portion interacts mainly with the more slightly open conformation of the C-terminal lobe of CaM leaving the other half to interact with the N-terminal lobe (Yamniuk and Vogel, 2004). The IQ motif takes on an α-helical conformation that also interacts through hydrophobic and electrostatic interactions with small hydrophobic patches and negatively charged amino acid scattered on the surface of apo-CaM (Zhang et al., 1995). The IQ motif is the most recognizable pattern among Ca^{2+}-independent proteins, however the IQ motif of some proteins can be also associated with Ca^{2+} bound CaM since they contain the same properties of being basic amphiphilic α-helices (Jurado et al., 1999). There are also a large number of Ca^{2+}-independent proteins that do not have the IQ motif.

1.1.3 Structural representation of CaM binding to target proteins

In addition to the Ca^{2+} dependency of CaM's target protein, CaM can bind to its target protein in a variety of different conformations that demonstrate the diversity of CaM. The most common and well studied conformation of CaM is where the terminal lobes wrap around the target protein as in the myosin light chain kinase (MLCK) (Figure 1.3b) (Ikura et al., 1992). This classical binding conformation is common in both Ca^{2+}-dependent and –independent groups because of the central linker region's ability to extend the accommodating distance of the terminal lobes (O'Neil and DeGardo, 1990).

<div style="text-align:center">a   b   c</div>
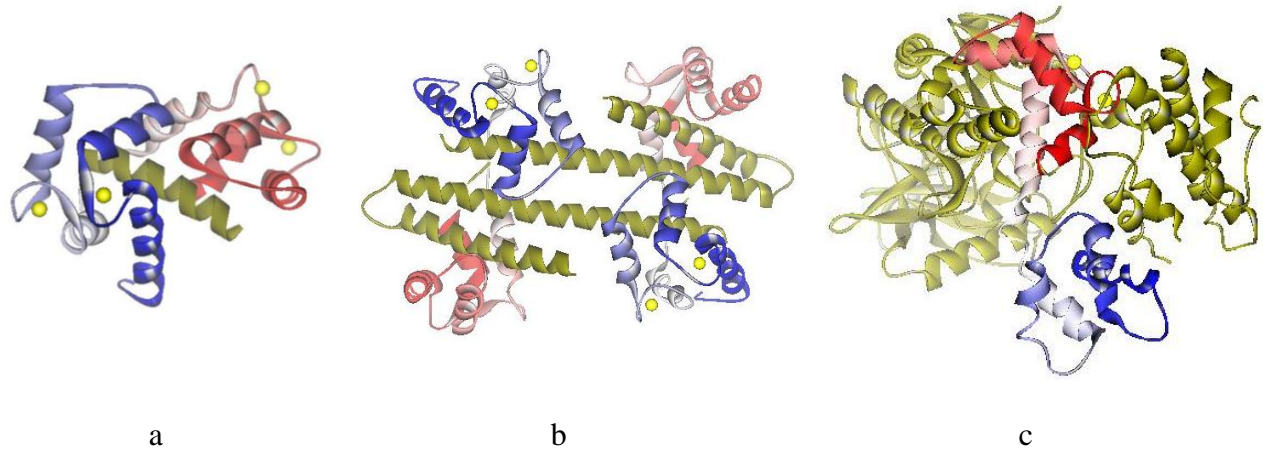
Figure 1.3. Calmodulin interactions with target proteins.
These figures show a few different modes of CaM interacting with the CaM-binding region of target proteins in (a) and (b) and with the whole protein in (c). The CaM is shown as the blue-red structure representing the N to C terminal with the Ca^{2+} ions as yellow spheres and the target protein in gold. CaM can interact with its target protein by wrapping around it like in (a) myosin-light chain kinase and (b) K^+-channel. In a unique case, the target protein wraps around CaM, (c) Oedema factor from *Bacillus anthraces*. (More information in text). Structures were made from PDB 2O5G, 1G4Y and 1k93 for a, b and c respectively using Accelrys DS visualizer.

More than one CaM can bind to its target protein such as in the case with potassium voltage gated channel. K^+-channels exist as a heteromeric complex (Figure 1.3b) and two CaM are required where the main interaction is through the hydrophobic patches in the Ca^{2+}-bound N-terminal lobe (Schumacher et al., 2001). The N-terminal lobe interacts with hydrophobic amino acids on the α-helix of one monomer and on another α-helix of the second monomer whereas the C-terminal lobe helps to stabilize the dimer by enclosing a third α-helix (Schumacher et al., 2001). The overall structure is an antiparallel dimer. A recent crystal structure of the exotoxin Oedema factor from anthrax adenylyl cyclase is one of the first to have a full structure of the protein bound to CaM (Figure 1.3c) (Drum et al., 2002). The study showed that CaM can interact with large areas of the target protein and initiate a large conformational change in the target protein that is required for protein activation (Drum et al., 2002). Aside from the three structures described, there are other ways that CaM can interact with its target protein.

On a molecular level, CaM can interact in an anti-parallel where the N-terminal lobe of CaM binds towards C-terminal end of the target protein and the C-terminal lobe to the N-terminal end or in a parallel manner where the terminals are orientated in the same direction (Yamniuk and Vogel, 2004). The determining factor for the orientation is which end of the target protein is more positively charged, since the outlet opening formed by CaM in its classical collapse wrapped around form is slightly more negative in the C-lobe than the N-lobe (Yamniuk and Vogel, 2004). In the majority of known peptides that bind to CaM, the N-terminus of the peptide is more positive and therefore binds to the C-terminal lobe of CaM in an antiparallel fashion. A few, such as the C-terminus of the peptide CaM kinase kinase, contain a larger positive charge and bind in a parallel fashion (Yamniuk and Vogel, 2004).

An important protein that CaM binds to and activates is nitric oxide synthase. Nitric oxide synthase is a good model to study since it includes two isoforms that are Ca^{2+}-dependent and one that is Ca^{2+}-independent. The information provided on nitric oxide synthase in the next section was available at the start of the study in fall 2007.

1.2 Nitric Oxide Synthase (NOS)

Nitric oxide ($\bullet$NO) is essential for controlling vital processes such as blood pressure through vascular dilatation, neuronal activity and as an immune response. This gaseous molecule is produced by the enzyme nitric oxide synthase (NOS) as a by-product of the conversion of L-arginine into L-citrulline (Figure 1.4). The catalysis of L-arginine uses electrons in a form of a hydride from the NADPH and molecular oxygen. For each L-citrulline and $\bullet$NO produced, 1.5 NADPH and 2 molecular oxygen are consumed (Griffith and Stuehr, 1995).
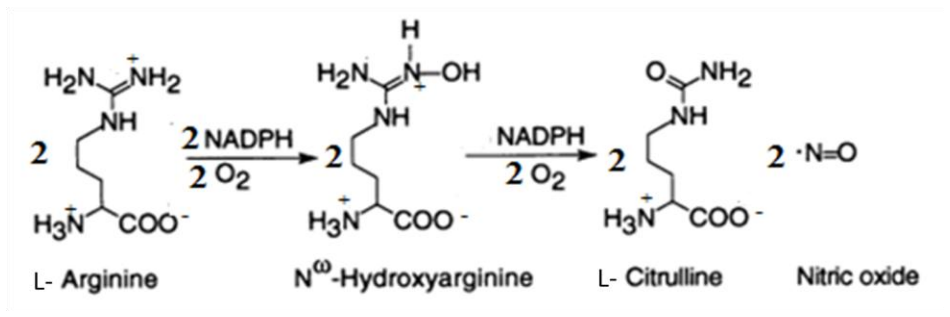
Figure 1.4. A reaction scheme of NOS where L-arginine is converted into L-citrulline.
The conversation of L-arginine to L-citrulline occurs as two mono-oxygenase reactions. The substrate L-arginine is converted first to the intermediate N-hydroxyarginine and then to the final product L-citrulline and nitric oxide using molecular oxygen and electrons from NADPH as a form of a hydride. Modified from Griffith and Stuehr (1995).

1.2.1 Isoforms of NOS

There are three isoforms of mammalian NOS that are unique in cellular function. These three isoforms are endothelial (eNOS), neuronal (nNOS) and inducible (iNOS) nitric oxide synthase found in endothelial cells, neuron cells and macrophage (Daff et al., 2001). The •NO produced by eNOS controls vascular dilation and blood flow where in nNOS, it is responsible for neurotransmission and for iNOS, •NO is used in the immune system as a defense against pathogens. The size of each isoform varies, with nNOS, eNOS and iNOS having a molecular weight of 165, 133 and 130 kDa respectively (Zhang et al., 2001). All three isoforms catalyze the reaction in Figure 1.4 and require CaM for activation, but differ from each other with respect to how they respond to calcium concentrations and structural regulation.

eNOS and nNOS are always expressed in the cytoplasm of the cell and are classified as constitutional NOS (cNOS). Since cNOS enzymes are always present, their enzymatic activity depends on increasing Ca^{2+} concentration in the cell and is active through Ca^{2+}-bound CaM, (Loscalzo and Vita, 2000). Therefore the cNOS enzymes are Ca^{2+}-dependent. iNOS, on the other hand, is made only when required and is controlled on the transcription level by cytokines in the

9

immune system. As soon as iNOS is transcribed, it can bind to CaM in the absence or presence of Ca^{2+} and therefore is said to be Ca^{2+}-independent (Griffith and Stuehr, 1995).

1.2.2 Mechanism of electron transfer in NOS

The overall structures of the isoforms are very similar with an oxygygenase domain and a reductase domain separated by a CaM-binding region (Figure 1.5). The oxygenase domain contains binding sites for the cofactor tetrahydroxybiopterin, the catalytic heme and the active site. The reductase domain accommodates the cofactors, NADPH and the two flavins, FAD and FMN.
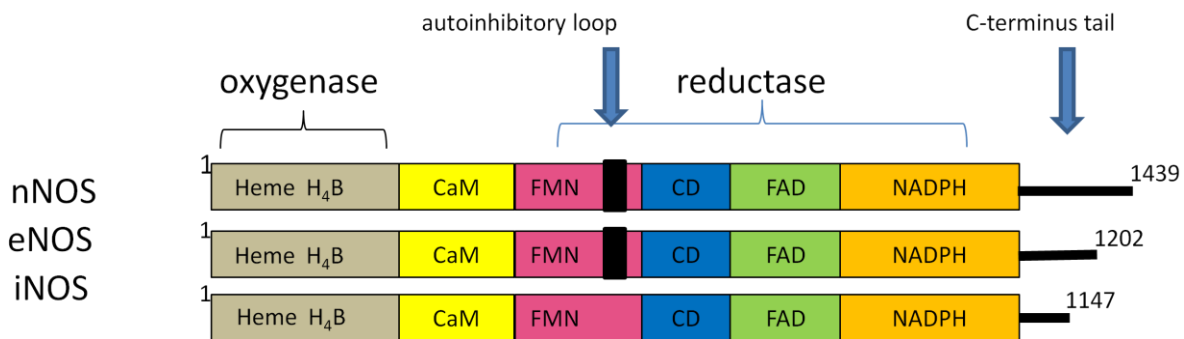
Figure 1.5. General domain alignment of the three isoforms showing the location of the regulatory elements and cofactors.
Shown are the oxygenase and reductase domains and the locations of the cofactors in each domain, which are the same for each isoform. The coloured boxes in the reductase domain are NADPH, FAD, CD (connecting domain) and FMN domains. The numbers represent the amino acid residue of each isoform. The autoinhibitory loop (AI) is in the FMN domain of the cNOS enzyme. The figure was modified from (Garcin et al., 2004)

The mechanism of electron transfer begins with NADPH passing two electrons in the form of a hydride ion to FAD to convert it to its reduced form, $FADH_2$. FMN remains in a stable-semiquinone state (FMNH•) in its resting stage, and is converted to its hydroquinone form, $FMNH_2$, when it receives an electron from $FADH_2$ or FADH• (Craig et al., 2002). The hydroquinone form of FMN then shuttles an electron to the oxygenase domain of the opposite

monomer where the electron acceptor is the heme. The first electron from $FMNH_2$ goes to reduce O_2 to produce a heme-dioxy and an electron from H_4B reduces the heme-dioxy to produce the reactive heme-oxy used to oxidize the L-arginine and produce the intermediate N-hydroxy-L-arginine (NOHA) (Figure 1.6) (Wei et al., 2008). A second electron from the $FMNH_2$ goes through the heme network to reduce the H_4B radical that was formed in the first step and the process with the heme-oxy is repeated to oxidize the NOHA to produce •NO and L-citrulline (Figure 1.6, step 6), (Wei et al., 2008, Stuehr et al., 2009).
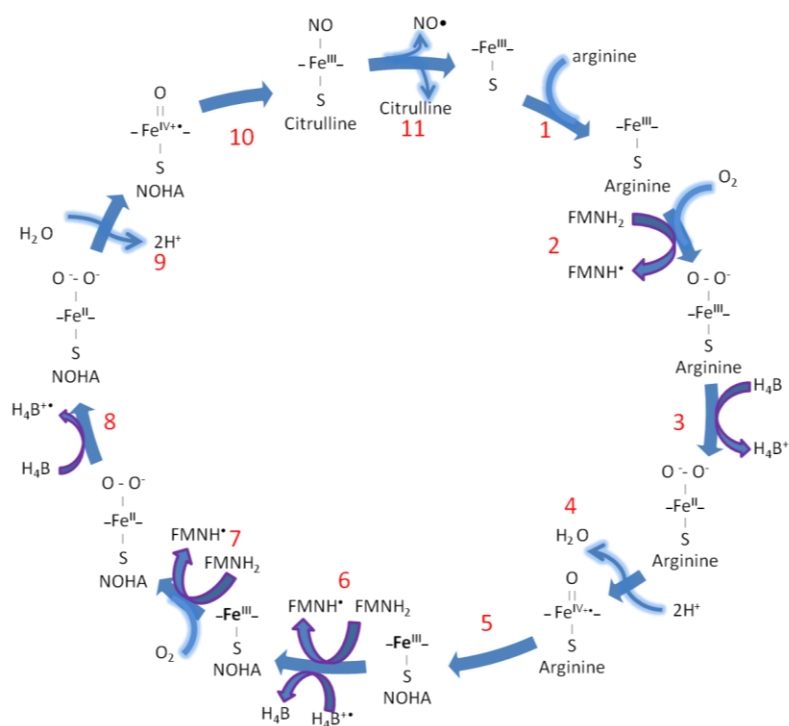
Figure 1.6. The reduction and oxidation of the catalytic ferric heme
The catalytic reaction of NOS starts with L-arginine being reduced by a reactive heme-oxy that is produced from steps 1 to 5 to make the intermediate N-hydroxyarginine (NOHA). The first two electrons are from $FMNH_2$ and H_4B. A freshly reduced $FMNH_2$ reduces $H_4B^{•+}$ back to H_4B allowing the reduction process of the NOHA (steps 7-10) to continue in the same manner as L-arginine but this time producing L-citrulline and •NO (steps 10-11). Modified from Wei (2008) and Stuehr (2009).

The majority of electron transfer occurs in the reductase domain using the cofactors NADPH, FAD and FMN (Figure 1.7). The electron flow through the reductase domain can be measured using enzymatic kinetic assays, such as the cytochrome c assay (Feelisch and Stamler, 1996). The cytochrome c assay measures the electron donating ability of the FMN, which is the cofactor responsible for the transfer of electrons to the heme in the oxygenase domain. Therefore results from cytochrome c assay are comparable to the FMN passing an electron to the heme.
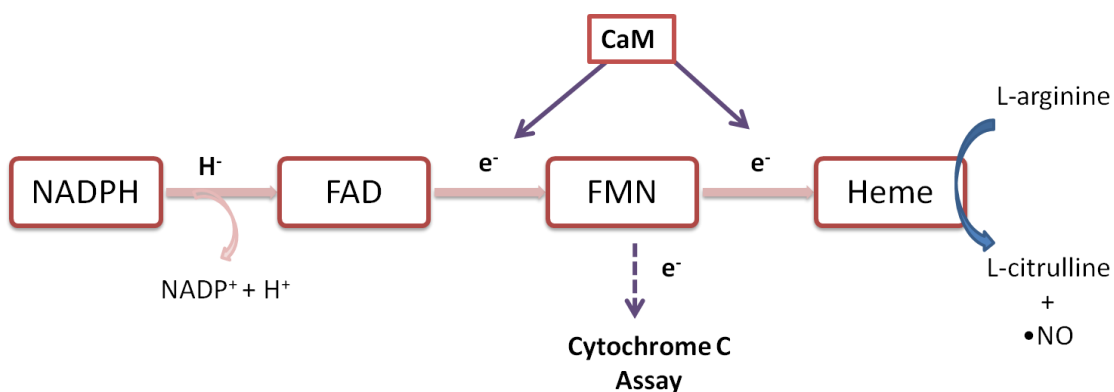
Figure 1.7. Schematic of electron flow in NOS with points of CaM control and cytochrome c assay.
The electron transfer from the reductase cofactors, NADPH, FAD and FMN to the heme can be monitored through the cytochrome c assay. The cytochrome c is able to accept electrons only from the FMN. In measuring the amount of electron transfer the cytochrome c accepts, a measure of the FMN transfer rate can be determined which would be equivalent to the transfer to the heme. CaM controls the flow of electrons between the flavins and in the transfer of electrons to the heme from the FMN. Modified from Spratt et al. (2007a).

The binding of CaM to the NOS enzymes increased the rate of cytochrome c reduction tenfold in the presence of CaM (Sheta et al., 1994). The binding of CaM also increased the electron flow through the reductase domain (Abu-Soud et al., 1994). Therefore CaM is an extremely important co-protein in the catalytic activity of NOS by allowing electron transfer between the two domains.

.

1.2.3 CaM-binding region of NOS

CaM is essential for the activation of the NOS isoforms. The binding affinity of CaM for each of the isoforms differs, with the highest binding affinity being iNOS, nNOS then eNOS (Ghosh and Salerno, 2003). The peptide sequence codings for the CaM-binding site of the three isoforms (Figure 1.8) follow the Ca^{2+}-dependent binding motif since they are composed of hydrophobic and basic amino acids arranged in a 1-5-8-14 pattern (Aoyagi et al., 2003).

```
           1       5       8      14
           ↓       ↓       ↓       ↓
nNOS  726  RRAIGFKKLA EAVKFSAKLM GGAM 749
eNOS  490  TRKKTFKEVA NAVKISASLM GTLM 513
iNOS  507  RREIPLKVLV KAVLFACMLM RKVM 530
```

Figure 1.8. Sequence alignment of the CaM-binding region of human NOS isoforms
Highlighted in red are the hydrophobic/non-polar amino acids and in bold are conserved amino acid in the isoforms. The nNOS and eNOS have more conserved amino acid than the iNOS but the iNOS contain more hydrophobic residues. The numbers on either side of the sequences indicate the amino acid residues. The numbers at the top with arrows indicate the amino acid used for characterizing the binding motif, 1-5-8-14.

The CaM binding region of the NOS isoforms was narrowed down by examining the NOS sequence for large hydrophobic patches that resemble the sequence of the Myosin light chain kinase (Venema et al., 1996). Using electrophoretic mobility shifts, they were able to determine the minimum amino acid sequence required to form a complex with CaM (Venema et al., 1996, Zhang et al., 1995). Mutation of key hydrophobic residues, Phe, Val and Leu to alanine resulted in no binding complex with CaM, therefore these residues play an important role in NOS binding to CaM (Venema et al., 1996). The sequence found that was required for CaM binding was residues 285-747, 492-510 and 501-531 for nNOS, eNOS and iNOS, respectively (Aoyagi et al., 2003, Matsubara et al., 1997, Venema et al., 1995, Venema et al., 1996, Zhang et al., 1995). When bound to CaM, the core amino acid residues between the anchoring

hydrophobic residues, Phe/Leu and Leu, are in an alpha helical conformation whereas the extra amino acids are in an extended conformation (Aoyagi et al., 2003, Ikura et al., 1992).

The cNOS peptide sequences are 54% identical whereas iNOS differs by 42 and 30% from nNOS and eNOS peptide respectively. Despite iNOS being classified as Ca^{2+}-independent, it does not follow the IQ motif but is more similar to the Ca^{2+}-dependent motif. However, the differences in iNOS from the cNOS enzymes are the presence of more hydrophobic amino acids and a much larger patch of them. The arrangement of the iNOS peptide in a α-helix conformation forms larger surface areas for hydrophobic interaction with CaM and accounts for the tight binding to CaM (Aoyagi et al., 2003). .

At the start of this study, available crystal structures were those of eNOS peptide (Aoyagi et al., 2003) and nNOS peptide (Valentine et al., 2006) bound to CaM (Figure 1.9) and both have CaM bound in the classic conformation. Both peptides form an α-helix and the phenylalanine in position 1 of the Ca^{2+}-dependent binding motif binds deep in the hydrophobic pocket formed by the methionine in the C-terminal lobe of CaM (Figure 1.9c&d). The other anchoring residue at position 14, a leucine, binds in the hydrophobic pocket of the N-terminal domain. Close inspection of the crystal structure shows that the nNOS peptide binds closer to the C-terminal lobe of CaM than eNOS, which may account for the tighter binding of CaM to nNOS.

a   b

c   d
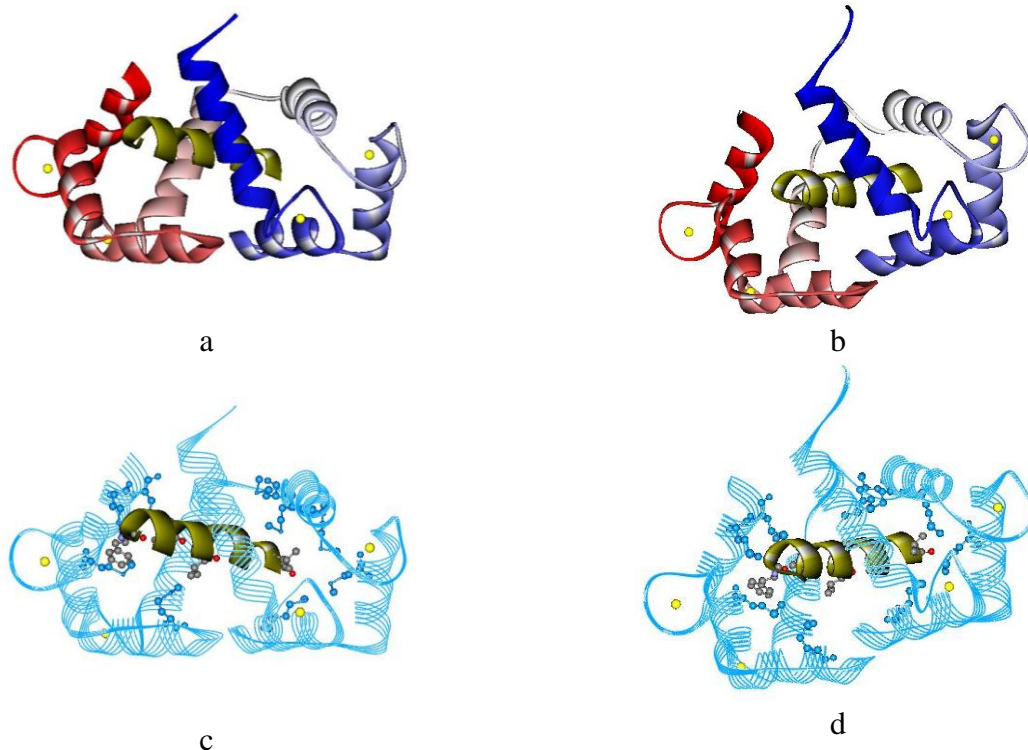
Figure 1.9. Comparison of the crystal structures of eNOS and nNOS
The peptides from the CaM binding region of eNOS (a) and (c) and nNOS (b) and (d) are shown in gold with the N-terminus end pointing out of page. (c) and (d) The amino acid residues involved in the 1-5-8-14 (Phe-Ala-Val-Leu) are shown as ball and stick figure. (a) and (b) CaM is shown as the blue and red structure, where blue represents the N-terminal domain and red represent the C-terminal domain in structure. In the blue line ribbon representation of CaM (c) and (d), the methionine residues of CaM are shown as blue ball and stick structure. The CaM orientation remains identical to that of (a) and (b) respectively. Structures were made from PDB 1N1W and 2O60 for eNOS and nNOS respectively using Accelrys DS visualize.

From the crystal structures, CaM binds to the cNOS enzyme in an anti-parallel manner which was verified by FRET studies that studied the orientation of the CaM binding lobe with respect to the terminus of the peptide (Spratt et al., 2007b). From the same FRET study, Spratt et al. (2007b) showed that the orientation for CaM bound to the iNOS peptide is also in an antiparallel orientation. The secondary structure of iNOS when bound to CaM is also known to be in an α-helix structure using circular dichroism (Yuan et al., 1998).

NOS chimeras using the iNOS oxygenase or CaM-binding region or reductase domain to replace those of nNOS resulted in chimeras that were more sensitive to Ca^{2+} concentration but

none obtained the full Ca^{2+}-independence of iNOS (Lee and Stull, 1998). This study was able to show that the CaM-binding site of iNOS as well as other regions in the reductase and oxygenase domains were also responsible for iNOS Ca^{2+}-independence (Lee and Stull, 1998).

1.2.4 Regulatory Elements

The domain alignment of the isoforms (Figure 1.5) indicates a unique regulatory element in the cNOS enzymes, the autoinhibitory loop, and a common element for all three isoforms, the C-terminal tail (Garcin et al., 2004). These regulatory elements in conjunction with CaM are able to regulate the enzyme activity of NOS.

The autoinhibitory (AI) loop is found only in the cNOS enzymes and contributes to their Ca^{2+}-dependent properties (Garcin et al., 2004, Daff et al., 1999). When the AI loop was removed in the cNOS, cytochrome *c* reduction for both eNOS and nNOS increased approximately twofold in the absence of Ca^{2+} when compared to that of the wild-type (Montgomery et al., 2000, Knudsen et al., 2003). Therefore the AI loop is responsible for some of the cNOS enzyme's Ca^{2+}-dependence. For eNOS in the presence of CaM, the •NO production increased by a factor of two when the loop was removed, indicating more electron transfer to the oxygenase (Knudsen et al., 2003). The insertion of the AI loop of eNOS into iNOS reductase domain caused the enzymatic activity to decrease to a third of the wild-type (Knudsen et al., 2003). In the crystal structure of the reductase domain, the loop lies within the FMN binding site and is thought to directly interact with CaM (Salerno et al., 1997, Garcin et al., 2004). It has been proposed that the AI loop locks FMN in its electron accepting position and when CaM binds, it is able to displace the AI loop and free the FMN domain to transfer electrons (Garcin et al., 2004). Clearly, the AI loop plays an important role in Ca^{2+} dependency of the cNOS enzymes restricting activity until there is a high enough concentration of Ca^{2+}-bound CaM.

The C-terminal tail is present in all three isoforms but varies in length with nNOS having the longest tail and iNOS the shortest. Studies by Roman et al. (2000) and Garcin et al. (2004) showed that when the C-terminus was truncated in the cNOS enzyme, the electron flow in the reductase domain increased significantly based on the measurement of the FMN reducing cytochrome C (Figure 1.7) and did so independently of CaM. nNOS and eNOS in the absence of CaM were reducing cytochrome c twenty-one and seven times more respectively than that of the wild-type enzyme with CaM bound (Roman et al., 2000). These results show that the C-terminal tail is responsible for restricting electron transfer in the reductase domain, since without the C-terminal tail, electron flow through the reductase domain increases. The C-terminal tail of cNOS is also required for maximum production of •NO since the •NO production of truncated cNOS in the presence of CaM compared to wild-type cNOS was reduced by 50% (Roman et al., 2000). Of note, the cNOS enzymes were able to produce low levels of •NO even in the absence of CaM. Therefore the C-terminal tail is proposed to play a role in the electron transfer between the two domains by locking the FMN cofactor in the electron accepting position (Craig et al., 2002). The binding of CaM is able to overcome the effects of the C-terminal tail. In iNOS, where CaM is always bound, the removal of the C-terminal tail resulted in an increase in cytochrome C reduction, an increase in •NO production and an increase in the flavins oxidization by molecular oxygen (Roman et al., 2000). Therefore the shorter C-terminal tail in iNOS is responsible for restricting electron flow in the reductase and for protecting the flavins from oxidation (Roman et al., 2000, Garcin et al., 2004).

In summary, the AI loop and the C-terminal, in addition to CaM, control the flow of electrons through NOS and are responsible for the unique Ca^{2+}-dependence and Ca^{2+}-independence of the NOS isoforms.

1.2.5 Structure of nitric oxide synthase enzymes

There are no full intact structures of any of the isoforms available due to proteolysis in the CaM-binding region and high mobility region, which makes crystallization difficult. Structural determination using nuclear magnetic resonance (NMR) is restricted since the NOS enzymes are so large. At the start of this study, available structures included the oxygenase domain of all three isoforms (Fedorov et al., 2003, Li et al., 2001, Matter et al., 2005, Fischmann et al., 1999, Rosenfeld et al., 2002), the reductase domain of nNOS (Garcin et al., 2004) and CaM bound to the CaM-binding region of eNOS (Aoyagi et al., 2003) and nNOS (Valentine et al., 2006) (Figure 1.10).
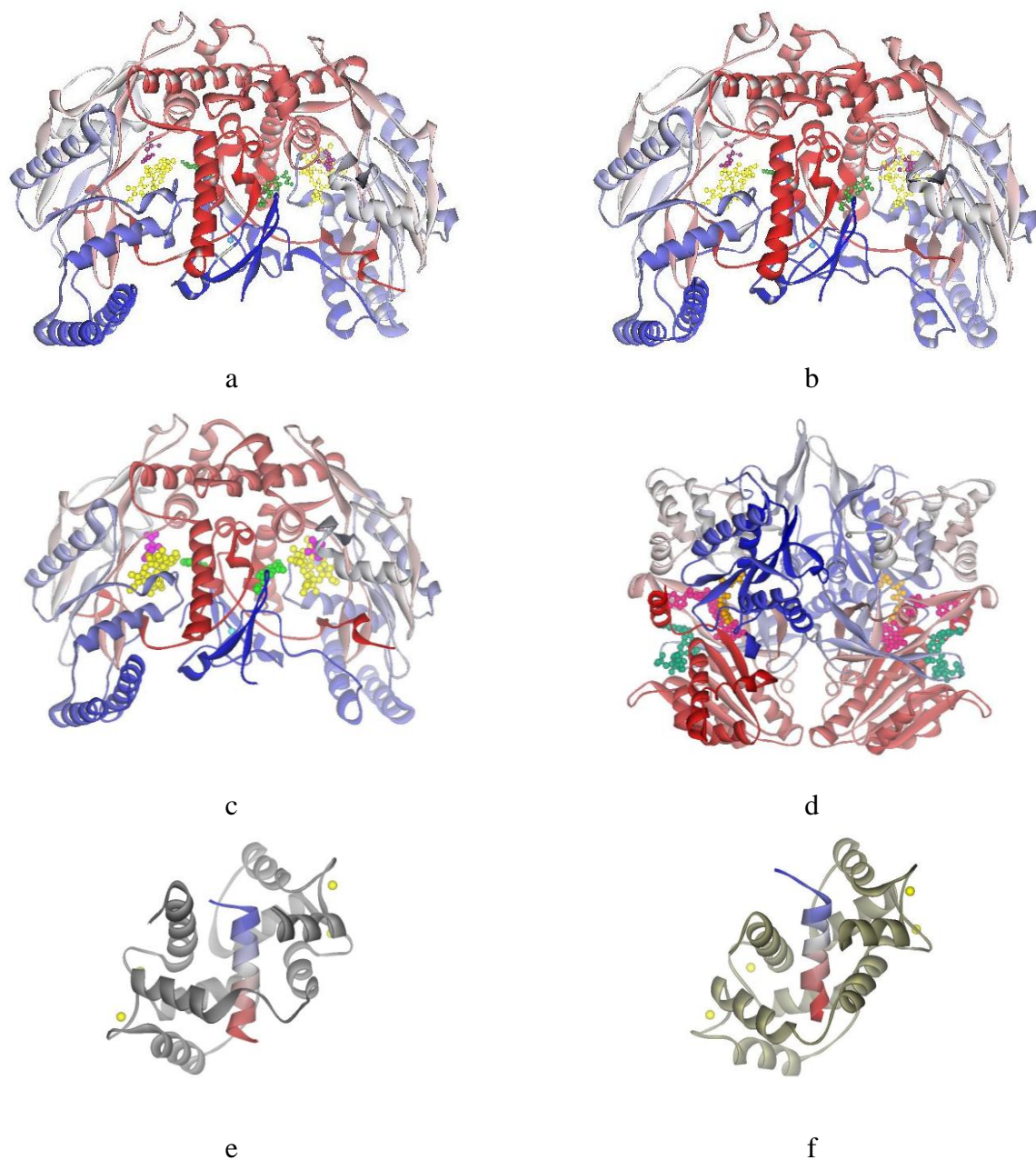
Figure 1.10. Solved crystal structures of nNOS oxygenase and reductase domains and the CaM-binding regions of nNOS and eNOS in complex with CaM

The crystal structure of (a) iNOS, (b) eNOS and (c) nNOS oxygenase domain dimer containing co-factors: heme and H_4B, and substrate L-arginine represented in yellow, green and pink ball and stick figures respectively. The cyan ball between the dimers is the Zn^{2+} ion. In the (d) nNOS reductase domain the cofactors: NADPH, FAD and FMN are represented in teal, magenta and orange, respectively. The Ca^{2+} ions in the CaM bound to the peptide from CaM-binding region of (e) nNOS and (f) eNOS are shown as yellow spheres. All NOS structures go from blue to red showing the N-C terminus. Structures 3E65, 1FOP, 1ZVL, 1TLL, 2O60 and 1NIW for (a), (b), (c), (d), (e) and (f) respectively were made using Accelrys DS visualizer.

19

The oxygenase domains (Figure 1.10a-c) of all three isoforms have very similar fold, and all three contain the heme and the H_4B situated near the dimer interface, which also contains a binding site for a zinc metal (Fischmann et al., 1999, Rosenfeld et al., 2002). The structure of the reductase domain of nNOS was the first to confirm that the reductase domain existed as a dimer, which is stabilized by salt bridges and hydrogen bonding in the interface (Garcin et al., 2004). The reductase domain as a dimer was first shown by Venema et al. (1997) using low-temperature SDS-PAGE gel to show the migration of dimers or monomers of the NOS isoforms. eNOS and nNOS both formed dimers in both oxygenase and reductase domains whereas iNOS formed a dimer in the oxygenase domain only. Therefore the iNOS reductase domain could be rearranged differently from the structure shown. As mentioned in section 1.2.3, cNOS are α-helical and bind in an antiparallel fashion such that the C-terminus and N-terminus of CaM interact closely with the N-terminus and C-terminus of the peptide respectively.

1.2.6 FMN swing model

The reductase domain of nNOS solved by (Garcin et al., 2004) gives significant insight into the orientation of the cofactors and regulatory elements. Based on the reductase crystal structure (Figure 1.11), the cofactors NADPH, FAD and FMN are within close proximity of each other for electron transfer. The FMN cofactor is tucked within the interface formed by the FAD and NADPH domain and is within ~4 Å from its electron donor, FAD (Ghosh and Salerno, 2003). In this position, the FMN cannot pass an electron to the heme in the oxygenase domain, which is proposed to be located 70 Å away, too far for electron transfer (Garcin et al., 2004).
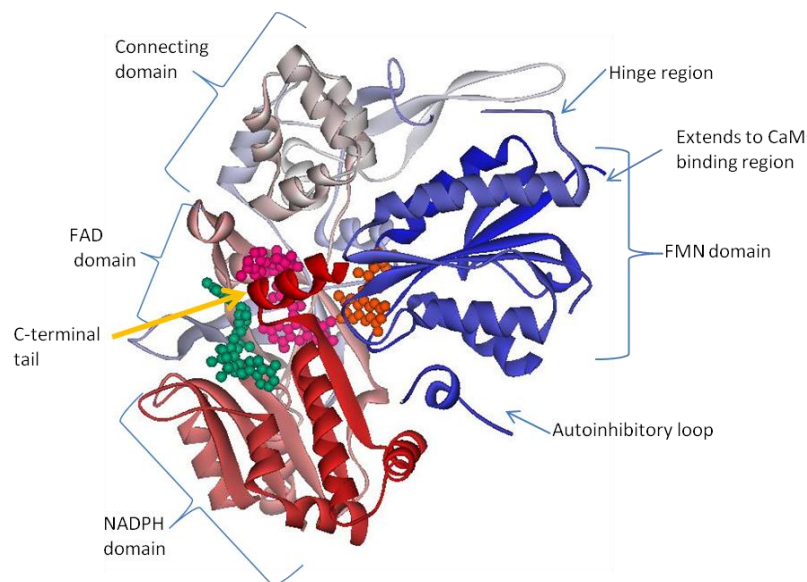
Figure 1.11. A closer look into the subdomains of the reductase domain using rat neuronal nitric oxide as the model.
The cofactors: NADPH, FAD and FMN are represented in teal, magenta and orange, respectively in each of their domains. Portions of the crystal structure are missing such as the autoinhibitory loop and the hinge region, most likely due to the region being highly mobile. Structure made from PBD 1TLL (Garcin et al., 2004) using Accelrys DS visualizer.

Based on the structures available it was proposed that subunit realignment and conformational changes had to occur to allow for the FMN domain to shuttle electrons from the FAD to the heme (Garcin et al., 2004, Ghosh and Salerno, 2003). Since CaM initiates the electron transfer between the two domains, CaM plays an important role in this dynamic process.

The hinge region (Figure 1.11) at the end of the CD and start of the FMN domain is flexible due to some portion of it being unstructured and acts as a pivot point allowing the FMN domain to swing back and forth between the FAD and heme (Garcin et al., 2004, Ghosh and Salerno, 2003). The surface of the oxgygenase domain near the heme interface is positively charged while the FMN domain is negatively charge allowing for a good docking area for the FMN domain (Garcin et al., 2004). Therefore the proposed model is similar to that in Figure 1.12, where the binding of CaM initiates the facilitation of electrons between the reductase and

21

oxygenase domain. The distance that the FMN cofactor is proposed to move is 55 Å to bring the

FMN within 15 Å of the heme (Garcin et al., 2004).
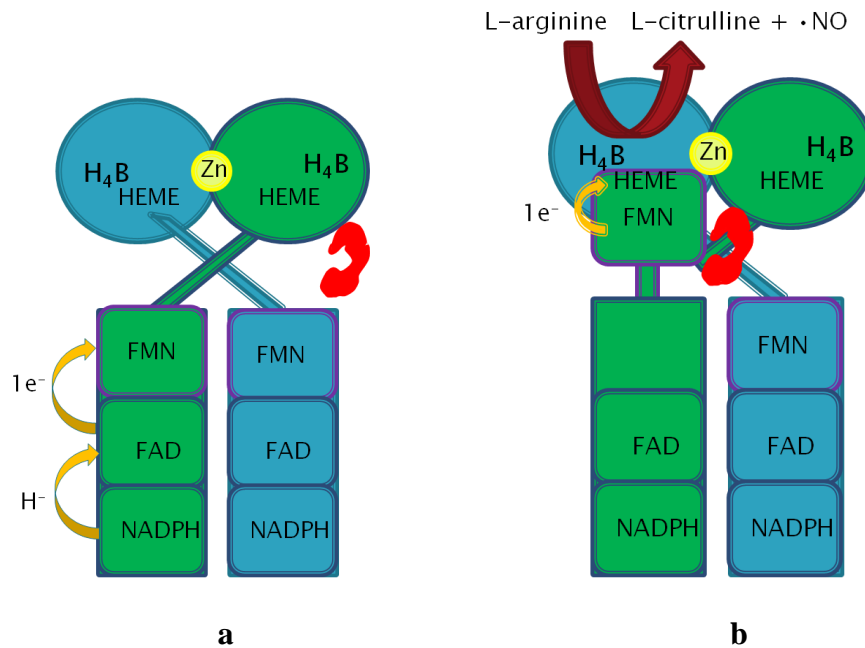
Figure 1.12. Cartoon representation of a NOS dimer showing the flow of electrons.
The ovals at the top of the figure represent the oxygenase domains and the rectangles are part of
the reductase domain. The long rectangle joining the oxygenase and reductase domains is the
CaM-binding region. CaM is shown as the red object. (a) The arrows show the flow of electrons
starting from NADPH to the FAD to the FMN domain in the reductase domain. (b) When CaM
binds, the FMN domain can swing up towards the heme in the oxygenase domain and pass an
electron. Figure was modified from (Daff et al., 2001, Garcin et al., 2004).

Exactly how CaM is able to initiate this process is still not fully understood. The binding

of CaM is known to displace regulatory elements in the cNOS enzymes and C-terminal tail but

structurally, it remains to be seen. Contrary to the cNOS enzymes, iNOS does not have the AI

loop and is Ca^{2+}-independent and may behave differently than the cNOS. Common to all three

isoforms is the requirement of CaM to initiate the electron transfer through a dynamic process.

1.3 Structure determination using nuclear magnetic resonance (NMR)

There are two main methods to determine 3-D protein structures; x-ray crystallography and nuclear magnetic resonance spectroscopy. Both methods have their advantages and disadvantages. X-ray diffraction of crystallized protein is useful for large proteins and can give high resolution structures; however, it requires the production of suitable single crystals. Crystallization of protein can prove to be difficult, especially with highly dynamic proteins or those prone to proteolysis, and misinterpretation can occur due to artifacts from crystallizing conditions and contacts between different molecules in the crystal. NMR is better suited for observing proteins that are highly dynamic. A drawback of NMR is that the large protein can complicate assignments and cause crowding in the spectra. Proteins under 30000 Da are the best candidates. As in crystallization, proteins for NMR need to be soluble at high concentrations (~0.1 – 1.0 mM). In addition, proteins for NMR structure determination require incorporation of isotopes such as ^{15}N and ^{13}C. (Brändén and Tooze, 1999).

NMR experiments detect the unique resonance frequencies of NMR active nuclei when they are exposed to rf-radiation inside a strong external magnetic field. Specific experiments can give rise to a set of signals that can be analyzed with respect to molecular structure, dynamics and protein interactions (Roberts, 1993a). Still a relatively new structural method, it has grown drastically due to the development of multi-dimensional NMR, advances in pulse sequences and modern equipment. For large proteins, two or higher dimensional NMR is required since one dimensional spectra yield poor peak dispersion and large overlap of signals. Two or higher dimensional experiments are based on correlation of two or more nuclei resonance frequencies of different elements through bond-bond or space and allow for the assignment of the correlation peaks to specific nuclei (Brändén and Tooze, 1999). The assignment of peaks has been made

23

easier with 3D and 4D NMR since they expand a 2D spectrum into another dimension and thus overlapping areas are separated into layers and the amount of crowded peak areas is reduced. Figure 1.13 shows the separation of a 2D NMR spectrum in the z direction, which correlates to another resonance frequency to resolve overlapping peaks and to allow for clear assignments.
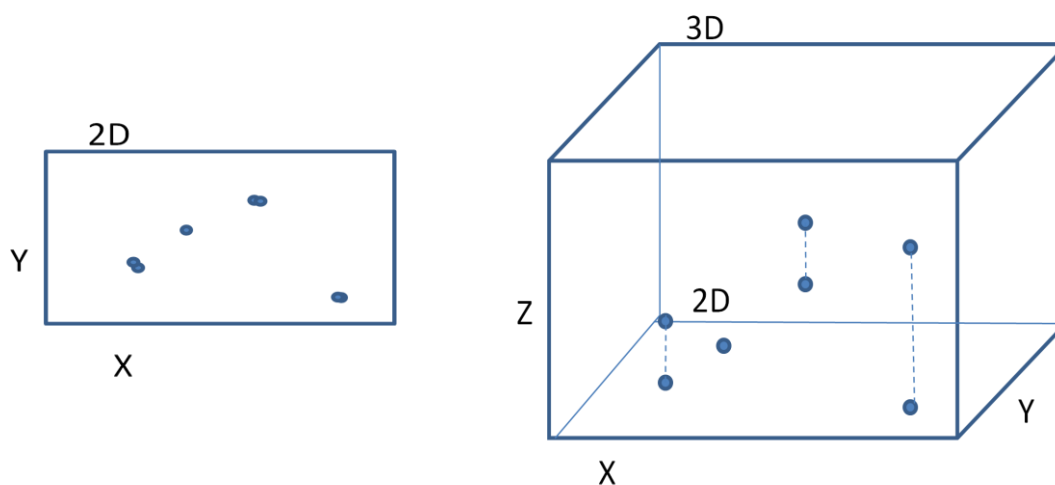
Figure 1.13. Overlapping peaks of 2D NMR spectrum resolved in the 3D NMR spectra.
In the 2D spectrum, the peaks represent correlation peaks between two types of nuclei: X and Y. There are areas where overlap occurs, which are resolved in the 3D spectra. In the 3D spectrum each of the X-Y correlation peaks is correlated to another nucleus, Z.

The main 2D spectrum utilized in our studies is the ^{1}H-^{15}N-heteronuclear single quantum correlation (HSQC) experiment. This experiment correlates nitrogens in the protein with their directly bound protons. This includes the side chain amides and those in the back bone of the amino acid with the exception of proline. The ^{1}H-^{15}N-HSQC is the first spectrum to be run since the peaks that appear in the spectrum represent a "finger print" of the protein. Assignments of the peaks in HSQC spectra cannot be accomplished without other 3D heteronuclear experiments. The 3D experiments are used to correlate ^{1}H-^{15}N peaks to the alpha or side chain carbons. A schematic of several 3D experiments is shown in Figure 1.14.
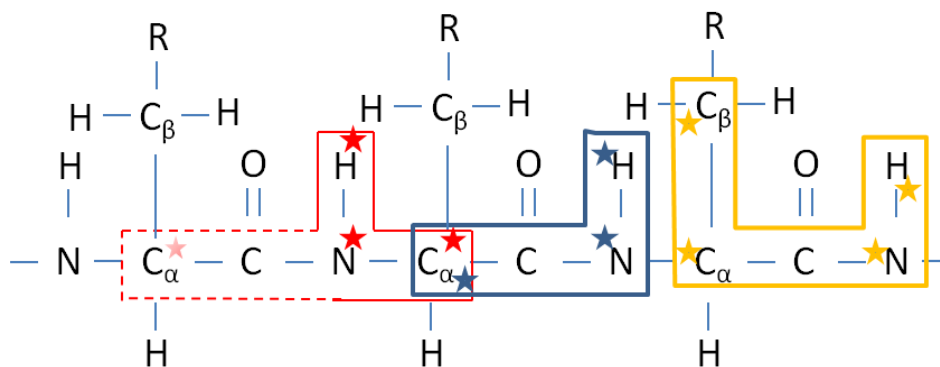
Figure 1.14. The path of magnetization in NMR 3D heteronuclear experiments
Three heteronuclear NMR experiments that help assign the backbone of the protein by expanding the ^{15}N-HSQC in the carbons direction. The stars indicate the nuclei that contribute to the peaks in the spectrum. The HNCA (red) allows for the assignment of the amide to the alpha-carbon of the same residue and to the previous alpha-carbon. The HNcoCA (blue) helps confirm which peak of the HNCA corresponds to the previous alpha-carbon to rule out any ambiguities. The CBCAcoNH (yellow) further confirms the previous alpha-carbon as well as confirming the correct amino acid residue by using some unique alpha and beta carbon patterns produced by different amino acids. (For NMR experiments see Appendix B)

Other experiments that are useful are total correlation spectroscopy (TOCSY), which is a 2D experiment that helps proton assignments in the side chain and correlates it to the alpha carbon and nuclear Overhauser effect spectroscopy (NOEs). The NOES gives interaction between proteins through space, as long as they are within 5 Å, allowing for the determination of secondary and tertiary structures. These experiments together allow for a family of structures that best fit the data and can demonstrate dynamics by the range of structures obtained.

1.4 Research Objectives

At the beginning of this investigation, there has been no full intact structure of any of the NOS isoforms. Available were the oxygenase domains, reductase domain of nNOS and the CaM binding region of the cNOS enzyme bound to CaM. All the information concerning the role of the protein in electron transfer came from these three-dimensional crystallographic studies of

cNOS enzymes. These studies indicated that the reductase domain had to undergo a significant structural rearrangement to allow for electron transfer to the oxygenase domain. iNOS is different from the other isoforms since it does not contain the AI loop, its proposed that its reductase domain does not form a dimer like the crystal structure of nNOS and is Ca^{2+}-independent (Venema et al., 1997). Very little structural information of iNOS is known since, at the start of this study, no three-dimensional structure of its reductase domain had been reported. Therefore the overall research objective was to investigate the dynamic properties of the FMN domain of iNOS and its association with CaM using nuclear magnetic resonance (NMR).

Since the FMN domain is about 30 kDa, the first phase of this investigation was to determine the three dimensional structure of CaM bound to the 24 amino acid iNOS CaM-binding region. This required the optimization of methods for expressing and purifying the isotopically labeled iNOS fragment.

Chapter 2 NMR investigation of calmodulin bound to the iNOS CaM binding region

2.1 Introduction

Three dimensional protein structure studies provide important insight into the function of proteins. These studies can confirm or contradict results from previous investigations, provide new insight into function and regulation and are useful for drug design. Since the dynamics of the FMN domain will eventually be investigated, NMR structural determination is the more logical and applicable method to use. In this investigation, we are trying to determine the structure of CaM bound to the iNOS CaM-binding region as a first step in the investigation of the structural dynamics of the FMN-CaM binding domain.

It is known that iNOS binds to CaM with the highest affinity out of the three isoforms. iNOS also differs from the other isoforms by being Ca^{2+}-independent and is always bound to CaM *in vivo*. At the initiation of this project, the structures for the other isoforms bound to CaM have been reported, but there has been no structure reported of the iNOS enzyme reductase domain.

To obtain the structure of the iNOS CaM-binding region bound to CaM using NMR requires two main processes. The first is to assign the NMR spectra of isotopically labeled wild type CaM bound to unlabeled peptide of the iNOS CaM-binding region. The second is to assign the spectra of the isotopically labeled iNOS CaM-binding region peptide bound to unlabeled CaM. Producing isotopically labeled proteins for NMR can be troublesome since they are expressed in bacteria grown in minimal media, and the final concentration required to conduct successful NMR experiments is 1.0 mM in a volume of 500 μL (Montelione et al., 2000). Some proteins, especially those that are highly soluble, can be produced in high yields as was the case

27

with CaM. However, others like the iNOS CaM-binding region are more problematic. Compared to the CaM-binding region of the other two NOS isoforms, the iNOS CaM-binding region has more hydrophobic amino acids and larger hydrophobic patches (Figure 1.8), which contribute to the peptide being insoluble (Matsubara et al., 1997, Spratt et al., 2006). Previous expression studies of the twenty-four amino acid long iNOS peptide in minimal media by Spratt (2008) using the poly-histidine tag vector, and the preliminary use of *New England Biolab* IMPACT-Twin intein self-cleavage expression system, have shown that the majority of the protein was insoluble. The protein in the inclusion bodies can be an advantage since a paper by Guo et. al. (2004) showed a successful extraction of their IMPAC-Twin expressed protein from the inclusion body using a step-wise dialysis method. For production of more soluble protein, lower induction temperatures accompanied by a prolonged period have been shown to increase solubility (Vaillancourt, 2003).

In this section the method for the expression and purification of a peptide from iNOS CaM-binding region (iNOS peptide) in minimal media was optimized to produce the required amount for NMR experiments. Included in the method was the attempt to refold proteins in the inclusion. The expression and purification process of isotopically labeled CaM had already been optimized by Spratt (2008). HSQC and 3D NMR experiments were run for the labeled iNOS peptide in complex with unlabelled wild-type holo-CaM to obtain spectra that are currently being assigned. The NMR spectra of isotopically labeled holo-CaM titrated with synthetically made iNOS peptide were completed prior to the start of this study and are also currently being assigned. So far, the EF hand regions have their backbone assigned where the central linker region of CaM bound to the iNOS CaM-binding region is still undetermined. The chemical shift difference when compared to the unbound CaM indicates that the N-terminal domain has a larger

shift than the C-terminal. For the assignment of the iNOS peptide, NOEs shows some α-helical properties.

2.2 Methods

2.2.1 Expression vectors

2.2.1.1 pTYB12 vector for the expression of iNOS CaM-binding region

Vectors for the production of the iNOS CaM-binding region were made by Spratt (2008). Spratt (2008) initially expressed the iNOS peptide using a poly histidine tag but that resulted in low yields due to protein insolubility. Expression trials in 2 L of minimal media for the poly-histidine tag fusion protein produced only 500 µL of 0.068 mM of protein. He then used the intein mediated purification with an affinity chitin-binding tag (IMPACT) system sold by *New England Biolabs* that had more promise in producing soluble proteins and a simpler purification process. This system consists of a chitin-binding domain (CBD) fused to the protein of interest via an intein linker (Figure 2.1).
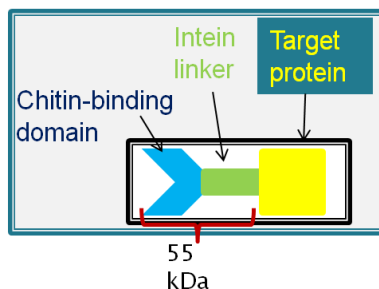
Figure 2.1. Representation of IMPACT fusion protein.
The IMPACT system adds a fusion tag that consists of the chitin-binding domain (cyan) and an intein linker region (green). The fusion tag is 55 kDa and attaches to the target protein via the intein linker.

The iNOS CaM-binding region was cloned into the vector pTYB12 that contains the CBD-intein and an ampicillin resistance gene using the restriction enzymes *NdeI* and *PstI*

(Figure 2.2). The restriction enzyme sites are located at the 3' end of the CBD therefore the iNOS peptide is attached to the fusion tag by its N-terminal. The cleavage process adds three extra amino acids to the N-terminus of the iNOS CaM-binding region peptide as shown by the underlined amino acids to produce a sequence of:

AGHMR PKRRE IPLKV LVKAV LFACM LMRK.

Shown in red are the amino acids of the iNOS CaM-binding region. A few additional amino acids, shown in blue, were from the *NdeI* cut site so the peptide that is produced is 29 amino acids long with a molecular weight of 3.4 kDa. Since CaM interacts with target proteins between the anchoring amino acid in 1-5-8-14 motif, extra amino acid would not interfere with CaM binding (Aoyagi et al., 2003).
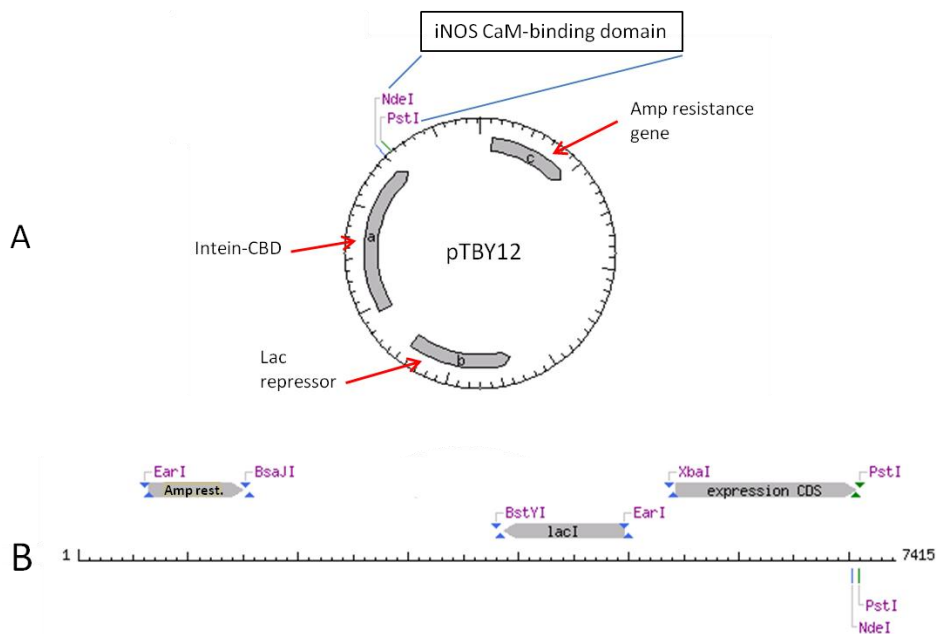
Figure 2.2. pTYB12 vector map showing restriction enzyme site for cloning in iNOS CaM-binding region.
The IMPACT pTBY12 vector contains an ampicillin resistance gene and an CBD-intein that was fused to the iNOS-CaM binding region by insertion at the *NdeI* and *PstI* sites. The location of the restriction enzyme sites allows for ligation of the fusion tag to the N-terminal of the iNOS peptide. (A) The pTBY12 in its circular form, showing the location of the important genes labeled using the red arrows. (B) A linear representation of the vector. Figure was made from *NEB* cutter using the vector pTYB12.

The recombinant protein is expressed using the recommended *E. coli* ER2566 cells (New England BioLabs, 2006). This strain contains the T7 RNA polymerase that is under the control of a *lacI* repressor which is released after the addition of IPTG to allow for the production of the protein. It also lacks *lon* and *ompT* proteases, which can degrade foreign or short proteins.

2.2.1.2 pET9d for the expression of Calmodulin

The vector pET9d (NOVAGEN) used to express the rat calmodulin was made by Newman (2003) by cloning in the CaM sequence using restriction enzyme sites, *NcoI* and *BaMHI*. The vector contains a kanamycin resistance gene that allows for selection of all cells containing the vector. There is no fusion tag associated with this vector since CaM can be easily purified using a single step purification process by using hydrophobic affinity column (see section 2.2.6.2). Competent cells BL21DE3 were used to express this protein.

2.2.2 Expression of protein in minimal media containing labeled isotope

2.2.2.1 Expression of the iNOS CaM-binding region using IMPACT-Twin system

Fresh ER2566 competent cells were prepared using a single colony to 1L of LB medium at 37°C until an OD of $0.5 - 0.7$ was reached. The pellet was harvested using sterile centrifuge bottles and spun down at 6000 rpm for 7 minutes at 4°C. The cell pellet was washed (resuspended and pelleted) twice with sterilized water, and once with 10% glycerol as the resuspension solution, respectively. The pellet was then resuspended in minimal volume, 1-2 mL, of 10% glycerol. The iNOS peptide vector was transformed in 40 µL of the fresh ER2566 competent cell by electroporation and plated on a selective agar plate containing 100 µg/mL ampicillin. An isolated colony was grown in 3 mL LB media that was used to inoculate the starter culture for minimal media growth.

Table 2.1 Minimal Media Ingredients

Components[a]	50 mL Starter Culture in 250 mL Flask	1 Liter Growth Culture in 4 L Flask	Final Concentration
10X M9 Salts Stock soln: 114 g $Na_2HPO_4 \cdot 7H_2O$ 30.0 g KH_2PO_4 5.0 g NaCl In 1 liter	5 mL	100 mL	1X
20% N[b]-NH_4Cl	250 µL	5 mL	0.1 % or 0.001 g/mL
40% C[b]-Glucose	250 µL	5 mL	0.2 % or 0.002 g/mL
2 M $MgSO_4$	50 µL	1 mL	2 mM
0.05% Thiamine	50 µL	1 mL	0.00005 % or 5 mg/mL
100 mg/mL Ampicillin	50 µL	1 mL	100 µg/mL
0.2 M $CaCl_2$	25 µL	500 µL	100 µg/mL
Starter Culture	0.5 mL[c]	5 mL[d]	

[a]For sterilization of the components of the media, M9 solutions were sterilized at $121^{o}C$ using an autoclave whereas all other solutions were filtered through a 0.2 µm pore sized filter. Method modified from (Roberts, 1993a)

[b]The ^{14}N- NH_4Cl and ^{12}C-Glucose was used in the minimal media sample with the exception of 1 L growth culture that were being prepared for NMR experiments where ^{15}N- NH_4Cl and ^{13}C-Glucose were used

[c]Starter culture from 3 mL LB media culture

[d]Starter culture from 50 mL minimal media culture

The expression trials of the desired protein were prepared in minimal media. Minimal media contains M9 salts (disodium hydrogen phosphate heptahydrate ($Na_2HPO_4 \cdot 7H_2O$), monopotassium phosphate (KH_2PO_4), sodium chloride (NaCl)), ammonium chloride (NH_4Cl), glucose, magnesium sulfate ($MgSO_4$), thiamine and antibiotic in concentrations according to Table 2.1 (Roberts, 1993a). 500 µL of the LB starter culture was used to inoculate the minimal media starter culture, which contained no isotopes, and which was allowed to grow in a shaker set to 160 rpm at $37^{o}C$ until an OD_{600} of about 0.6 was reached (about 6 hours). The 1 L minimal media was prepared in 4 L flasks and inoculated with 5 mL of the minimal media starter culture that had been pelleted and resuspended in M9 salt.

a) Inclusion body production

For the production of proteins in the inclusion bodies 2 L of minimal media was used to express the recombinant protein. The cells in the minimal media samples were induced at an OD_{600} of 0.9 (about 11 hours) with 1 mM IPTG. Induction period was found to be optimal for 6 hours at $37^{o}C$ at which point the cell pellet was collected, frozen using dry ice and stored at $-80^{o}C$.

b) Soluble protein production

For the production of soluble protein 4 L of minimal media growth was required. Protein production was induced at $15^{o}C$ with 1 mM of IPTG when the OD_{600} reached 0.9 – 1.0 (about 11 hours). The induction period was extended to 20 hours at which point the cells were either harvested and used immediately or rapidly frozen using dry ice and stored at $-80^{o}C$ until purification.

2.2.2.2 Expression of recombinant CaM

Calmodulin was expressed and purified as previously reported in Spratt (2008) with the expression in minimal media and was uniformly labeled with ^{15}N or doubly labeled with ^{15}N and ^{13}C isotopes. The purification was performed by phenyl-sepharose affinity chromatography according to Gopalakrishna and Anderson (1981).

2.2.3 Purification of recombinant proteins

2.2.3.1 iNOS CaM binding domain

a) Protein extraction from inclusion bodies

The pellet obtained from a 2 L minimal media growth that produced insoluble protein in section 2.2.2.1.1 was refolded according to Guo et al. (2004). The protocol used for the iNOS peptide was very similar with a few changes but a drip-wise reduction of urea was used. The cell

pellet was homogenized in intein lysis buffer (20 mM Tris pH 7.5, 500 mM NaCl, 1 mM $CaCl_2$ and 0.01% Triton X-100) in a 1:10 (1 gram: 10 mL of buffer) ratio and lysed by passing solution through an emulsifier. After centrifugation the insoluble fraction in the pellet portion was washed twice with the buffer A (50 mM Tris pH 7.0, 500 mM NaCl) which contained 0.1% Triton X-100 and 1 M urea. This step ensures that any small cell debris such as cell wall and small non-essential proteins were removed. The remaining pellet was resuspended in an extraction buffer (50 mM Tris pH 7.0, 500 mM NaCl, and 8 M urea) by shaking at room temperature for 4 hours. Any remaining precipitate was removed by centrifugation and the supernatant was transferred to dialysis tubing with the addition of wild-type CaM. The dialysis tubing was placed in a large mixing chamber that contained 1.5 liters of the base buffer with 7 M urea at $4^{o}C$. The concentration of urea was reduced by 1 M every 18-20 hours by dripping in buffer A until a concentration of 1 M was reached. Before each addition of buffer A, the solution in the dialysis bag was spun down to remove any precipitate. After dialysis in buffer A with 1 M urea, the sample was dialyzed in the 1.5 L of refolding buffer (20 mM Tris-HCl pH 7.0, 500 mM NaCl, 0.2 mM GSH, 0.02 mM GSSG and 0.5 M L-Arg) for 18 hours. The refolded solution was then purified as usual via chitin bead column (section 2.2.3.1 b)

b) Purification of soluble IMPACT recombinant protein

The pellet obtained from 4 L of minimal media culture growth was resuspended in the intein lysis buffer (20 mM Tris pH 7.5, 500 mM NaCl, 1 mM $CaCl_2$ and 0.01% Triton X-100) in a 1:10 (1 gram: 10 mL of buffer) ratio with the addition of unlabelled CaM for a final concentration of 10 μM. This suspension was passed through an Avestin EmulsiFlex-C5 homogenizer set at 17000 psi twice and after centrifugation the supernatant was passed through a

10 mL bed volume of chitin beads. Prior to the addition of the supernatant, the chitin bead column was equilibrated with ten times column volume of wash buffer (20 mM Tris pH 7.5, 500 mM NaCl, 1 mM CaCl$_2$). Contaminating proteins were removed by washing the column after the addition of supernatant with another ten times column volume of wash buffer at a rate of 2.0 mL/min. For elution of the protein, the column was incubated at room temperature in cleavage buffer (20 mM Tris pH 8.5, 500 mM NaCl, 1 mM CaCl$_2$, and 50 mM DTT) for 48 hours. Under these reducing conditions the Asn454 located at the C-terminus of the intein tag is induced to form a succinimide and break the bond between the iNOS CaM-binding region and the fusion tag (New England BioLabs, 2006). Elutions were collected in 2 mL fractions by passing a pH 8.5 wash buffer through the column. 3 µL samples from each fraction were used to run on a Tris-tricine gel (section 2.2.4) to determine which fractions contained the iNOS CaM-binding region. The appropriate fractions were pooled together, concentrated down to 1 mL using the Viva spin column with the 3 kDa cut off and then run through a Superdex 75 10/300, 500 µL at a time. The wash buffer used for the chitin bead was also used in the gel filtration process. The fractions containing the desired protein were concentrated down and were quantified using the Lowry method with CaM as the standard. Protein purity was confirmed by a final SDS-PAGE gel and mass spectrometer analysis before the sample was either prepared for NMR analysis or stored at -80°C.

2.2.3.2 Isotope labeled CaM

The purification of CaM utilizes the hydrophobic properties of CaM when it binds to Ca^{2+} in a one step chromatographic process using the phenyl-sepharose affinity column. The lysis process is similar to that of iNOS CaM binding domain but the lysis buffer used was composed of 50 mM MOPS pH 7.5, 100 mM KCl, 1 mM EDTA and 1 mM DTT. The

purification process was carried out according to the methods in (Gopalakrishna and Anderson, 1981), with buffer 1 being 50 mM Tris-HCl pH 7.5 and 1 mM $CaCl_2$ and the elution buffer containing EDTA instead of EGTA. The eluted fractions were checked for the presence of CaM by scanning the solution from 250 to 300 nm looking for the signature peak pattern of CaM due to its lack of tryptophan and large ratio of phenylalanine to tyrosine (Klee et al., 1980).
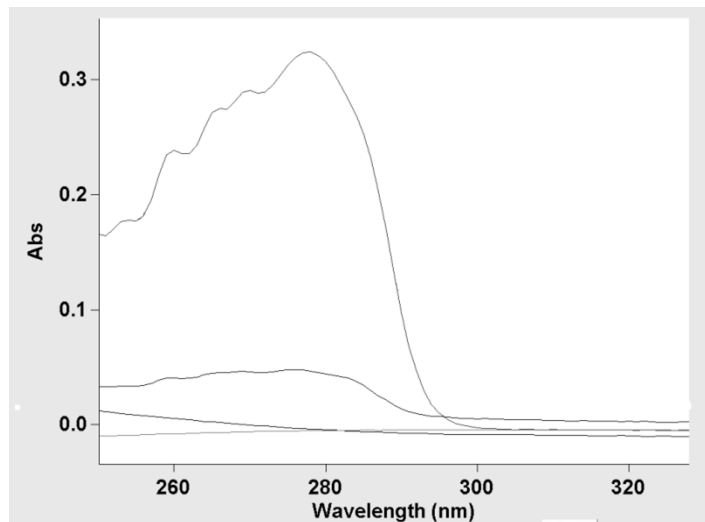
Figure 2.3. Spectroscopic analysis of CaM.
Characteristic spectrum of purified CaM showing peaks at 277, 269, 265, 259 and 253 nm.

The fractions that contained the CaM peaks were pooled together and dialyzed in buffer overnight using 6-8 kDa cut off dialysis tubing. A Lowry was performed to determine the concentration of CaM produced. The protein solution was separated into 500 µL aliquots, frozen on dry ice and stored at $-80^{\circ}C$.

2.2.4 Tris-Tricine SDS-PAGE Visualization of iNOS CaM-binding region

The protein produced from pTBY12 vector (CBD-intein-iNOS peptide) was about 60 kDa but after cleavage from the fusion tag, the peptide portion was only 3.7 kDa, which was too small to monitor using SDS-PAGE analysis. However, during the purification process the CaM that was added would associate strongly with the iNOS peptide and provide a way of detecting

the presence of the iNOS peptide. Therefore the presence of CaM would also indicate the presence of the iNOS peptide. Although CaM is 17 kDa and can be seen on a traditional SDS-PAGE gel, the 16.5% acrylamide Tris-tricine gel was used because it allows for the detection of small proteins as low as 4kDa. The method used was a modified version of Schagger and von Jagow (1987).

A 3x separating gel buffer was made with the final concentration of 3 M Tris-HCl pH 8.43, 0.3% SDS, 3% glycerol. For 12 mL the separating gel that is enough to make two 15x15 cm gels, 4 mL of the 3x separating buffer, 6.6 mL of 30% acrylamide and 1.4 mL of water was used. This ratio produces a final concentration of 33.3% of 3x buffer and 16.5% of acrylamide.

For stacking gel, the 3x stacking buffer consisted of 3 M Tris-HCl pH 8.43 and 0.3 % SDS. For two gels, a 5 mL preparation used 1.67 mL of 3 x stacking buffer, 0.66 mL of 30% acrylamide and 2.67 mL of water to make a final concentration of 33.33% of stacking buffer and 4 % acrylamide. A little (10 μL) saturated bromophenol blue was added to this mixture to make the lanes visible when loading samples. In both cases, the solution was also degassed and polymerized by using 10% APS and TEMED.

Added to the sample were 4x loading dye (40% glycerol, 250 mM Tris-HCl pH 6.8, 8% SDS, 0.04 mg/mL bromophenol blue, 5% βME and 100 mM EDTA) to make a final concentration of 1x. The samples were boiled, loaded and run at 200 volts while the gel apparatus was attached to a water cooling system. Gels were run for about 2 hours or until the blue front reached the bottom.

2.2.5 Sample preparation for NMR investigation

Samples being prepared for NMR require a special experimental buffer made up of salt and 10% D_2O which provides the signal that is used to adjust the magnetic field so the sample is

within the lock frequency of the spectrometer (Roberts, 1993b, Wüthrich, 1986). The labeled iNOS peptide bound to unlabelled CaM was in Tris buffer therefore a buffer exchange was required. The 15 mL 3 kDa Viva spin column was loaded with the protein solution and concentrated to 500 µL. The flow through was discarded and the NMR buffer (100 mM KCl, 10 mM $CaCl_2$, 0.2 mM NaN_3, pH 6.0 no adjustment) was added to the 10 mL mark on the spin column and concentrated again to 500 µL, which takes about two hours. This process was repeated five times to ensure all traces of Tris buffer were gone. For the final spin, the sample was concentrated down to 450 µL so that a 50 µL addition of D_2O can be added for a final 10% D_2O composition. The final concentration was 500 µL of ~1.4 mM protein. The sample was transferred into a NMR 5 mm, 7'' sample tube and stored at 4^oC until required for NMR experiments.

2.2.6 NMR experiments

2.2.6.1 iNOS CaM-binding region

The prepared sample was analyzed on Bruker 600 or 700 MHz NMR spectrometers according to standard setting for the specific NMR experiment being run (see Appendix B). All experiments were run by Dr. Thorsten Dieckmann. NMR experiments performed on the peptide were ^{15}N-HSQC, HNCA, CBCAcoNH and a 3D ^{15}N-NOESY. The spectra were visualized and assignments were made using Computer Aided Resonance Assignment (CARA) version 1.8.4, 2007 (Keller, 2004).

2.2.6.2 CaM

The expression and purification of CaM produced peptide-free holo-CaM but we wanted the structure of CaM bound to the iNOS peptide. To obtain the complex, synthetically made

iNOS peptide (Sigma-Aldrich) was titrated into the CaM NMR solution. The synthetic iNOS peptide was prepared by dissolving the powdered peptide in water to produce a concentration of 1 mM, aliquot into 200 μL and 100 μL fractions in 0.5 mL Eppendorf tubes and then lyophilized. For the best 1:1 binding ratio, the HSQC spectrum was used to monitor the disappearance of the free CaM peaks and the appearance of the peaks of CaM in complex with iNOS CaM-binding region with each addition of lyophilized iNOS peptide. The final saturated sample was used to run the rest of the NMR experiments using the Bruker 600 or 700 MHz NMR spectrophotometers. The majority of the NMR experiments for the CaM protein were acquired in 2007 and 2008 by Dr. Thorsten Dieckmann and Don Spratt (PhD, 2008, UW). The experiments obtained for isotope labeled CaM bound to the unlabeled peptide of the iNOS CaM-binding region were ^{15}N-HSQC, HNCA, CBCAcoNH, HNCOCA, HCcH-TOCSY and NOESY. The spectra were visualized and assignments were made using Computer Aided Resonance Assignment (CARA) version 1.8.4, 2007 (Keller, 2004).

2.2.6.3 NMR spectra assignment strategy

The assignment of a protein starts with the ^{15}N-HSQC spectrum which shows the backbone amide protons and nitrogen as well as the amides in the side chains of amino acids. The spectrum is opened in *SynchroScope* using CARA. *SynchroScope* is one of the viewing modes in CARA that allows for easy backbone assignments. The main window contains the HSQC spectrum where at each hydrogen-nitrogen chemical shift, corresponding carbon peak(s) in the 3D experiments will be shown in the strip window. In the strip window of *synchroscope* mode, 3D NMR experiments such as HNCA, HNcoCA and CBCAcoNH can be opened. These 3D NMR experiments correlate the H-N of amino acid 'i' on the HSQC to a C_α of amino acid 'i', 'i-1' and C_β of 'i-1' respectively (Figure 2.4A). The assignments started with giving each

observed peak in the HSQC spectrum a peak number. In the strip window, HNCA will give two peaks with one larger than the other. The larger peak was assigned to the $C_{\alpha(i)}$ and the smaller one to the $C_{\alpha(i-1)}$. The $C_{\alpha(i-1)}$ assignment was confirmed using the HNcoCA and CBCAcoNH spectra since they both contain the $C_{\alpha(i-1)}$. The CBCAcoNH also contains the peaks for $C_{\beta(i-1)}$. Once all possible peaks were assigned to H, N, $C_{\alpha(i)}$, $C_{\alpha(i-1)}$ and $C_{\beta(i-1)}$, the HNCA is opened in *StripScope* mode where each strip shows the $C_{\alpha(i)}$ and $C_{\alpha(i-1)}$ peaks assigned in *SynchroScope* which correspond to a backbone amide. Connecting residues can be determined by finding best matches of $C_{\alpha(i)}$ and $C_{\alpha(i-1)}$ in different strips by using the function *select strips - all best precursor* or - *all best successor*. This function aligns all best carbon chemical shifts for the preceding or subsequent amino acid (Figure 2.4B). By using amino acid residues in the sequence that have unique carbon chemical shifts, such as alanine, glycine and threonine, the peak number can be assigned to an amino acid residue. These unique amino acids are then used as starting points for assigning peaks to the protein sequence; and knowing the expected amino acid adjacent to these unique amino acids can confirm whether preceding or subsequent amino acid assignments were correct.
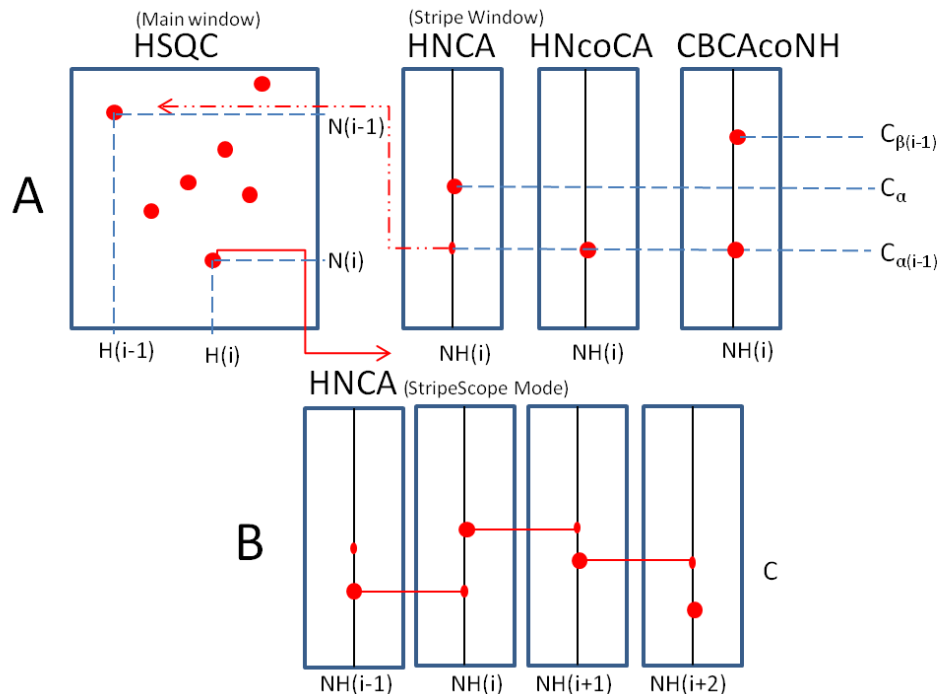
Figure 2.4. Sequential assignments of protein using HSQC, HNCA, HNcoCA and CBCAcoHN.

In the CARA, using the *SynchroScope* viewing mode to open the (A) HSQC spectrum in the *main window* that contains correlation peaks between the nitrogen and proton of an amide. For each NH correlation, there are correlation peaks to the alpha carbons of the same amide amino acid and of the preceding amino acid and the beta carbon of the preceding amino acid as seen in the 3D experiments, HNCA, HNcoCA, and CBCAcoNH. These 3D experiments are viewed in the *Strip window* of *SynchroScope*. (B) The preceding carbon shift can be used to determine the NH correlation peak it belongs to. This process was done using the *StripScope* viewing mode by lining the preceding carbon peak of one strip to the alpha carbon of another strip.

After the backbone assignments, the side chains of the amino acids are assigned using the ^{15}N-edited HSQC-TOCSY and NOESY spectra. These two spectra are opened in *PolyScope* mode where you can move along the nitrogen planes in the strip window. At each nitrogen plane that corresponds to an amide backbone, the protons of the side chain (TOCSY) and protons that are within 5Å (NOESY) will be present as well as cross peaks between neighboring amide protons. The assignment of the TOCSY peaks will help identify which peaks in the NOESY are intraresidue and which are interresidue.

2.3 Results

2.3.1 iNOS CaM-binding region expression and purification

During the optimization of the intein recombinant iNOS CaM-binding region (intein-iNOS peptide), various induction temperatures and protein expression periods were tested to determine their effect on expression level and solubility. Results of the different trials and the final yield of iNOS CaM-binding region are summarized in Table 2.2.

Table 2.2. Summary of expression and purification results of iNOS CaM-binding region.

Purification conditions	Growth Conditions in Minimal media	Yield^a from 2L of minimal media
Intein-iNOS peptide	37°C growth, 22°C induction for 6 hrs	~ 0.025 mM (750 µL)
Intein-iNOS peptide with CaM in lysis step	37°C growth, 22°C induction for 6 hrs	~ 0.03 mM (750 µL)
Refolding of intein-iNOS peptide drip-wise	37°C growth, 37°C induction for 6 hrs	None No self-cleavage
Intein-iNOS peptide with CaM in lysis step	37°C growth, 22°C induction for 12 hrs	~ 0.42 mM (500 µL)
Intein-iNOS peptide with CaM in lysis step	37°C growth, 15°C induction for 20 hrs	~ 0.84 mM (500 µL)

^{a} Yield was determined using the Lowry method using wild-type CaM as the standard

Results that will be shown are those of the refolding of intein-iNOS peptide using the drip-wise dialysis method and the method used to produce the iNOS CaM-binding region for NMR experiments.

a) Results of purification iNOS peptide from inclusion bodies

The pellet yield of insoluble protein was 2.4 grams from 2 L of minimal media enriched with ^{15}N and ^{13}C isotopes. Protein expression was good producing a large portion of protein in the insoluble fraction in the pellet after cell lysis and centrifugation. 8 M urea was able to solubilize the majority of the pellet with a small precipitate remaining, which was separated from the solution and used to compare to the soluble fraction. CaM was added during the 8 M urea

step to help keep the iNOS peptide portion soluble once protein started to refold, since it was seen that, at 7 M urea, a large amount of protein precipitated out of solution. During the drip-wise dialysis to reduce the urea concentration, precipitate that formed was removed before continuing to the next concentration. Samples from the precipitate and soluble fraction showed the proportion of soluble to insoluble intein-iNOS peptide was reduced during each step of the drip-wise urea reduction (Figure 2.5). By the refolding buffer less than a quarter of the protein was found to be soluble. The soluble protein that remained in solution was used to load onto the chitin bead column but during the elution process, no proteins were eluted.
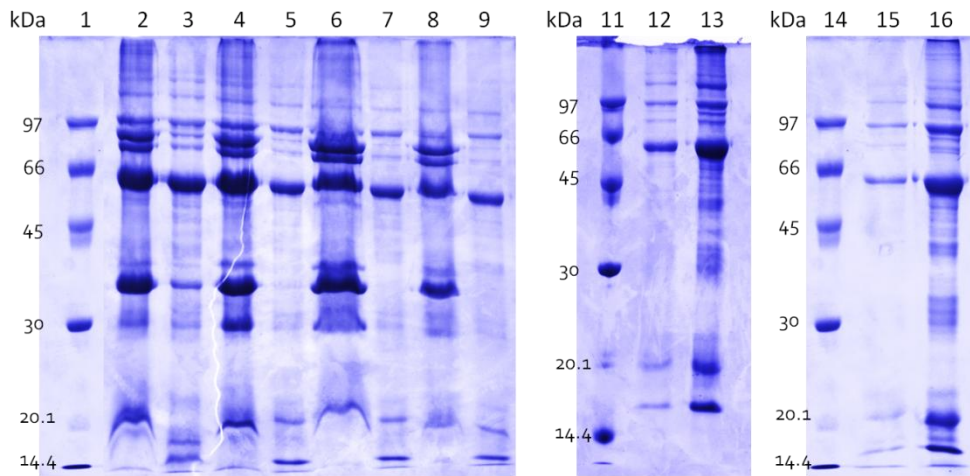
Figure 2.5. 10% SDS-PAGE of intein-iNOS peptide solubility in refolding process.
The solubility of sample during the drip-wise dialysis was analyzed by comparing the supernatant and the pellet at each urea concentration since precipitate was seen at each dialysis level. Samples from supernatant collected at 8, 6, 4, 2 and 1M urea as well as in the refolding buffer (lanes 2, 4, 6, 8, 12 and 15 respectively) were compared to their soluble counterpart (lanes 3, 5, 7, 9, 13 and 16 respectively). Low molecular marker (Lanes 1, 11 and 14) was used to monitor the position of intein-iNOS peptide located at ~60 kDa and CaM at 17 kDa.

b) Result for intein-iNOS soluble protein

A 2 L culture of fresh ER2566 competent cells transfected with pTYB12-iNOS peptide vector when grown in minimal media enriched with ^{15}N and ^{13}C isotopes resulted in a cell pellet weighing 8.2 grams. Since 4 L was used for final protein prep, the total cell pellet was 16 grams.

The expression of the CBD-intein-iNOS peptide protein was confirmed running a 10% SDS-PAGE (Figure 2.6) prior protein purification. The CBD-intein-iNOS peptide protein can be seen faintly at about 60 kDa in the red box after 22 hours of induction, which was not observed at time 0.
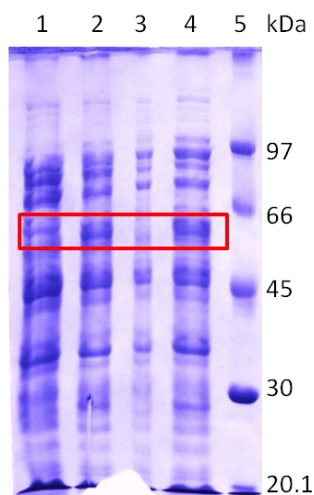
Figure 2.6. 10% SDS-PAGE gel used to confirm expression of CBD-intein-iNOS peptide protein
Two flasks were grown for each 1 L culture. Lanes 1 is the uninduced and lane 2 is the induced sample after 20 hours from flask 1. Lanes 3 and 4 are the uninduced and induced (taken at 22 hours) respectively for flask 2. For lane 1 to 4, gel sample was prepared using the pellet from 1 mL sample taken from the minimal media at time 0 and 20 hours and resuspended in 2x SDS sample loading buffer according to the sample's optical density at 600 nm. For every 1 OD_{600} of the sample, the pellet was resuspended in 100 μL of loading buffer. Lane 5 is the low molecular marker to monitor the expression of the ~60 kDa CBD-intein-iNOS peptide.

During the purification process, samples from each step were taken and run on a 10% SDS-PAGE gel as a precautionary measure before continuing with the purification process. The majority of proteins produced were soluble, which was verified by the large band at 60 kDa in the supernatant lane of Figure 2.7. The CBD of the fusion tag was tightly bound to the chitin beads since no CBD-intein-iNOS peptide band was seen in the flow through or wash (Figure 2.7, lane 5 and 6). Excess CaM that did not bind to any iNOS CaM binding domain can be seen in the

flow through lane at ~17 kDa. Therefore the CaM found in the subsequent steps of the purification process is CaM that is tightly bound to the iNOS CaM-binding region.
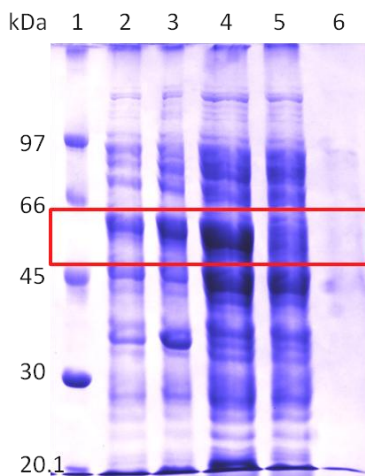
Figure 2.7. 10% SDS-PAGE analysis of the purification process for the CBD-intein-iNOS peptide before eluted from the chitin beads.
The monitoring of protein content of each step during the purification. 1) Low molecular marker. 2) Homogenized sample taken after the resuspended cell pellet was lysed by the emulsifier. After centrifugation samples were taken from 3) the pellet and 4) the supernatant to determine the solubility of the protein. 5) Sample taken from flow through when the supernatant was passed through the chitin column. 6) Sample from the flow through during the wash step of the column. The CBD-intein-iNOS peptide band is located at ~60 kDa, red box, and can be seen in the lanes 2,3, and 4. The ~17 kDa CaM band is seen slightly in the lanes 2-5. This gel shows the CBD-intein-iNOS peptide was soluble and adhered to the chitin column.

Elution of the CaM-iNOS peptide by incubating the column in 50 mM DTT initiated the self-cleavage of the intein as described in section 2.2.3. Each 2 mL fraction was run on a 16.5% Tris-Tricine SDS-PAGE gel (Figure 2.8) to determine which fraction contained the CaM-iNOS peptide. In an SDS-PAGE analysis, the complex formed by the CaM and the iNOS peptide dissociates under the denaturing condition and is seen as two separate bands, 17 kDa for CaM and ~4 kDa for iNOS peptide (Figure 2.8). According to the gel analysis of the elution process, about 5 mL eluted material was collected before the CaM became visible and continued to increase. Three additional fractions (not shown) were collected after the gel in Figure 2.8 since

fraction 12 indicated proteins were still present on the column. Fraction 3 to 15 were pooled and

concentrated using the Viva spin column with a 3 kDa molecular weight cut off.
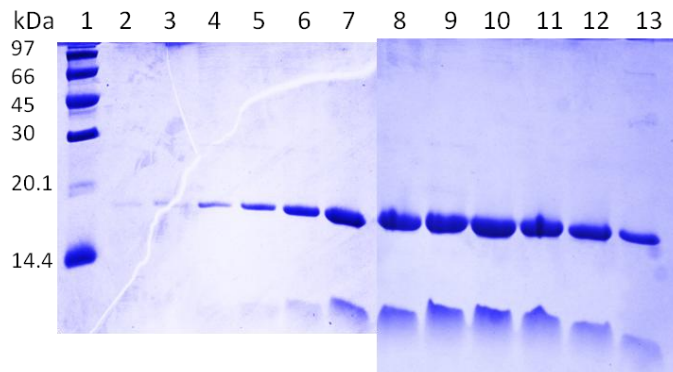
Figure 2.8. 16.5% Tris-tricine SDS-PAGE analysis of the eluted fractions from the chitin column.
The fusion protein bound to the chitin resin was incubated for 48 hours in buffer containing 50 mM DTT. Elution of the CaM-iNOS peptide was monitored using SDS-PAGE. 3 µL from each of the 2 mL fraction were used for the analysis. Lane 1 is the low molecular marker. Lane 2-13 represents fractions 1-12 respectively. All fractions contained some CaM-iNOS peptide, but fractions in lane 3-13 were pooled as well as additional 6 mL eluted after lane 13.

Some large molecular weight contaminants were seen in Figure 2.8, fraction 12 and were

more apparent when the sample was concentrated; therefore gel filtration was employed to

remove these proteins as well as residual DTT that was not removed during the concentration

step. The results from the gel filtration chromatography step using Superdex 70 10/300 are

shown in Figure 2.9. A SDS-PAGE (Figure 2.9B) run on samples eluted from the gel filtration

column showed that the large molecular proteins were removed and a mass spec was run to

further confirm purity of the sample (Appendix A).
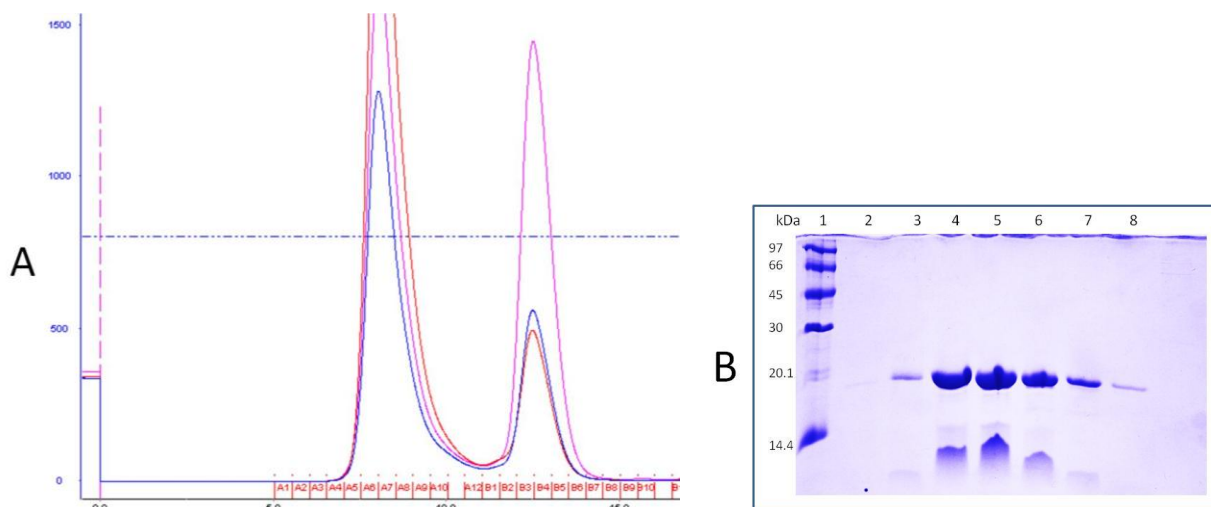
Figure 2.9. 16.5% Tris-Tricine gel analysis of the CaM-iNOS peptide elution from the Superdex 75 10/300 column.
The A) gel filtration profile zoomed in to where the high molecular weight protein contamination and CaM-iNOS peptide peaks were eluted off the column. The high molecular contaminants were eluted off in fraction A5 to A10 and the elution of the CaM-iNOS peptide was eluted in fractions B3 to B5. B) A gel was run on to the CaM-iNOS peptide fractions, B2-B9, and it was found that fraction B4-B8 had the majority of the protein.

Protein quantification by the Lowry method showed a yield of 500 µL of 1.2 mM of iNOS that was purified from a culture grown in 4 L minimal media. A buffer exchange into NMR sample solution describe in section 2.2.5 was performed and placed in NMR sample tube and stored at 4°C.

2.3.2 NMR spectra and assignments

2.3.2.1 iNOS CaM-binding region

The NMR experiments for the ^{13}C and ^{15}N isotopically labeled iNOS peptide in complex with unlabelled CaM were run on the Bruker 700, except for the ^{15}N-edited HSQC-NOESY which was run on the Bruker 600. The first experiment was the HSQC (Figure 2.10) which was checked for the possible twenty-seven peaks produced by the peptide. About twenty-six peaks were seen with some minor background peaks. Using the assignment strategy laid out in section

2.2.5.3, there were many H-N peaks that had no corresponding peaks in the HNCA or CBCAcoNH spectra. On the other hand, there were a few peaks, 16 and 31, that had corresponding carbon peaks in the 3D spectra but had a very weak peak in the HSQC. These peaks have yet to be assigned to an amino acid residue in iNOS peptide and could be artifacts or background noise.
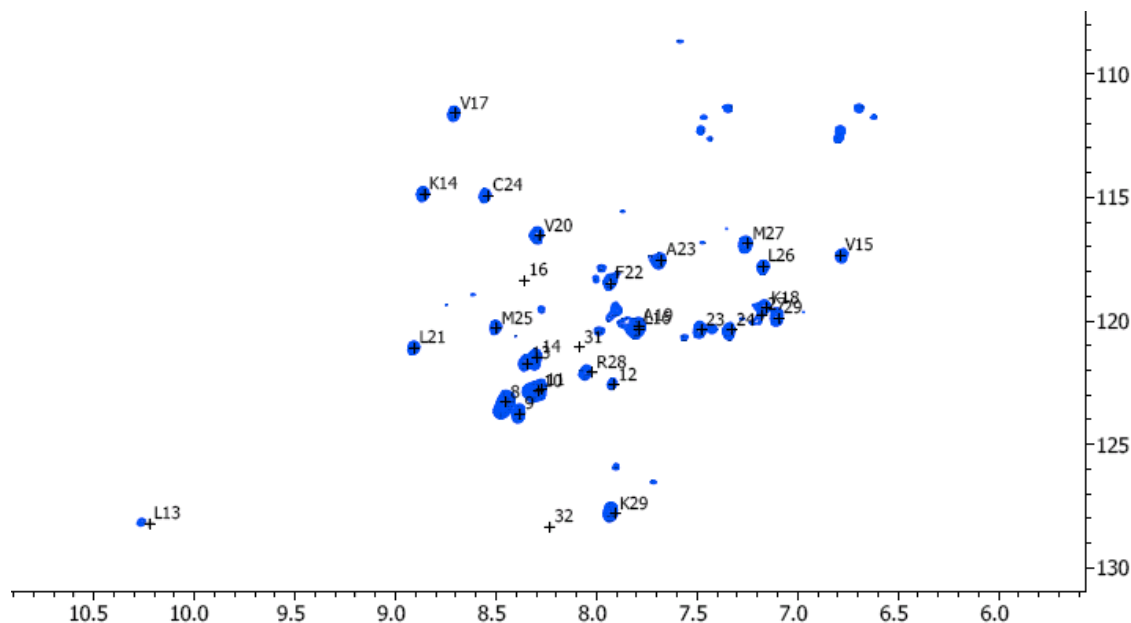
Figure 2.10. HSQC spectrum of isotopically labeled iNOS peptide bound to unlabeled CaM with partial peak assignments.
This spectrum was run on the Bruker 700. The iNOS peptide peak assignments show the correlation between the amide and their proton. Most peaks have been assigned to amino acid residues but the few with just numbers have not yet been assigned or have some ambiguities. The spectrum was analyzed using the CARA NMR visualizer.

For the peak numbers that were assigned to amino acid residues, three-dimensional NMR experiments such as HNCA and CBCAcoNH were used to determine connection between sequential residues of the iNOS peptide. The NOESY spectrum was able to confirm these backbone assignments (Figure 2.11). However, the connection through space (NOE) between the side chain and of other side chains that are within 5 Å could not be confidently assigned without the TOCSY spectrum. Comparing the NOESY spectrum with the bond coupling in the TOCSY

spectrum enables the intermolecular peaks in the NOESY to be identified. The intermolecular peaks can help in the prediction of secondary structures. In the NOESY spectrum some noticeable NOE peaks could be determined (Figure 2.11) belonging to the proton of the alpha carbons. The peaks of these alpha carbons are correlated with the amide proton two and three residues away which are characteristics of an α-helix (Roberts, 1993a, Wüthrich, 1986). But to confirm these assignments and to further the assignments of the side chains, a TOCSY is required.
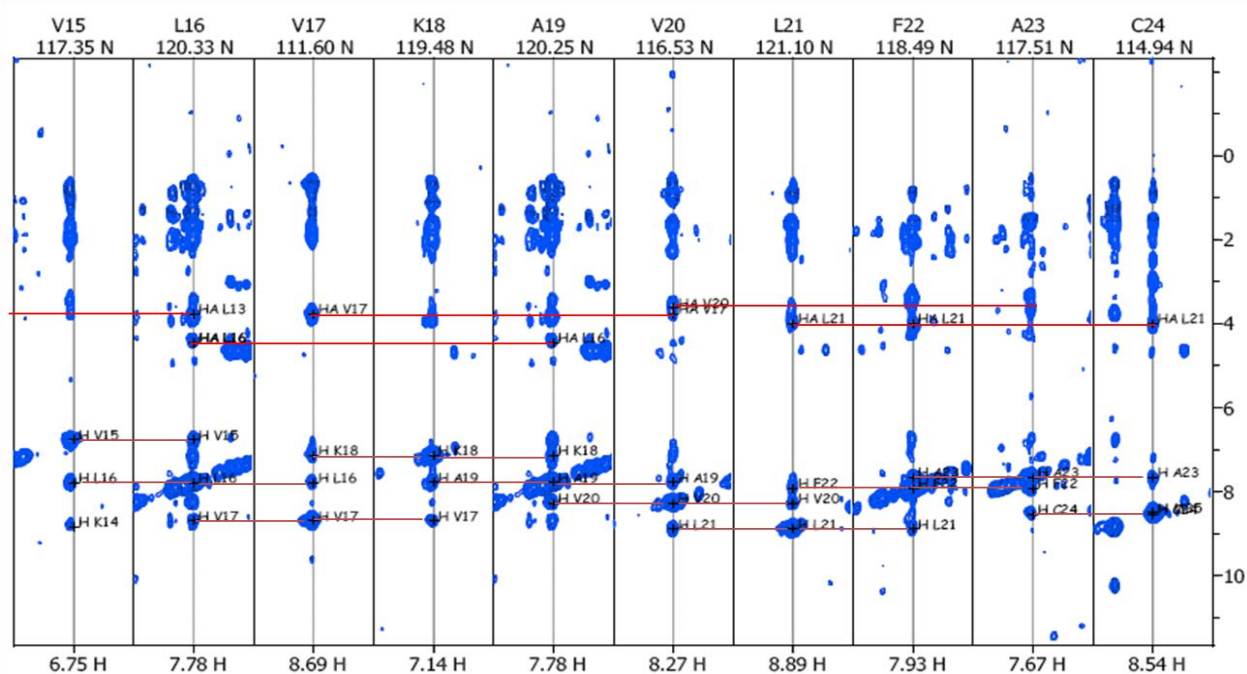
Figure 2.11. ¹⁵N-NOESY of iNOS peptide.
NOESY stripes of sequential amino acid Val15 to Cys24 of the iNOS peptide. The connection between the amide protons of the previous and successor residue are shown in the bottom half of the spectra in burgundy. Protons of the alpha carbon of a few residues, L16, V17 and L21, are assigned. The peaks corresponding to these protons appear in the spectrum of amino acids that are three residues away, shown in the upper portion of the spectrum in red. These NOE connections are indicative of an α-helix secondary structure.

The backbone assignment of amino acid residues assigned for the iNOS CaM binding domain at this point is highlighted in red below and is also shown in Figure 2.12. Lists of chemical shifts are presented in Appendix C.

<u>AGH</u>MR PKRRE IPLKV LVKAV LFACM LMRK

Figure 2.12. Crystal structure iNOS CaM-binding region showing the assigned amino acids.
The structure shows the helical conformation of iNOS CaM binding region, glutamine 512 to lysine 531. Highlighted in red, are the amino acids that have been assigned (leucine 515 to lysine 531). Structure made from the newly published crystal structure of iNOS FMN-CaM binding region bound to CaM, PDB 3HR4 using Accelrys DS visualize v2.5.1.

The sequence of the iNOS peptide begins at the blue amino acid residues. Therefore the majority of the amino acids that have not been assigned belong to the extra residue left over from the intein cleavage and the *NdeI* cut site. The unassigned region (blue residues) is separated from the assigned region by a proline. Because a proline does not have an amide peak in the HSQC, the sequential backbone assignment strategy using the information from the assigned area could not be used. Nitrogen-proton correlation for the unassigned residues could not be assigned to a peak number in the HSQC. Free peak numbers, which are peaks not assigned to an amino acid residue on the iNOS peptide, did not show backbone connection with other free peak numbers. Therefore these residues remain unassigned to a peak number.

2.3.3 NMR experiments on CaM

The titration of the synthetic iNOS peptide of the CaM-binding region into the CaM NMR solution used two 200 μL and one 100μL of the 1 mM lyophilized peptide stock. The HSQC spectrum ran after each addition showed the progress of the titration by comparing the disappearance and appearance of the free CaM peaks and peptide bound CaM peaks respectively

(Figure 2.13). Once all the free CaM peaks were gone, it can be assumed a 1:1 binding ratio (pink peaks) had been met.

a

b
Glycine 33

c
Arginine 137
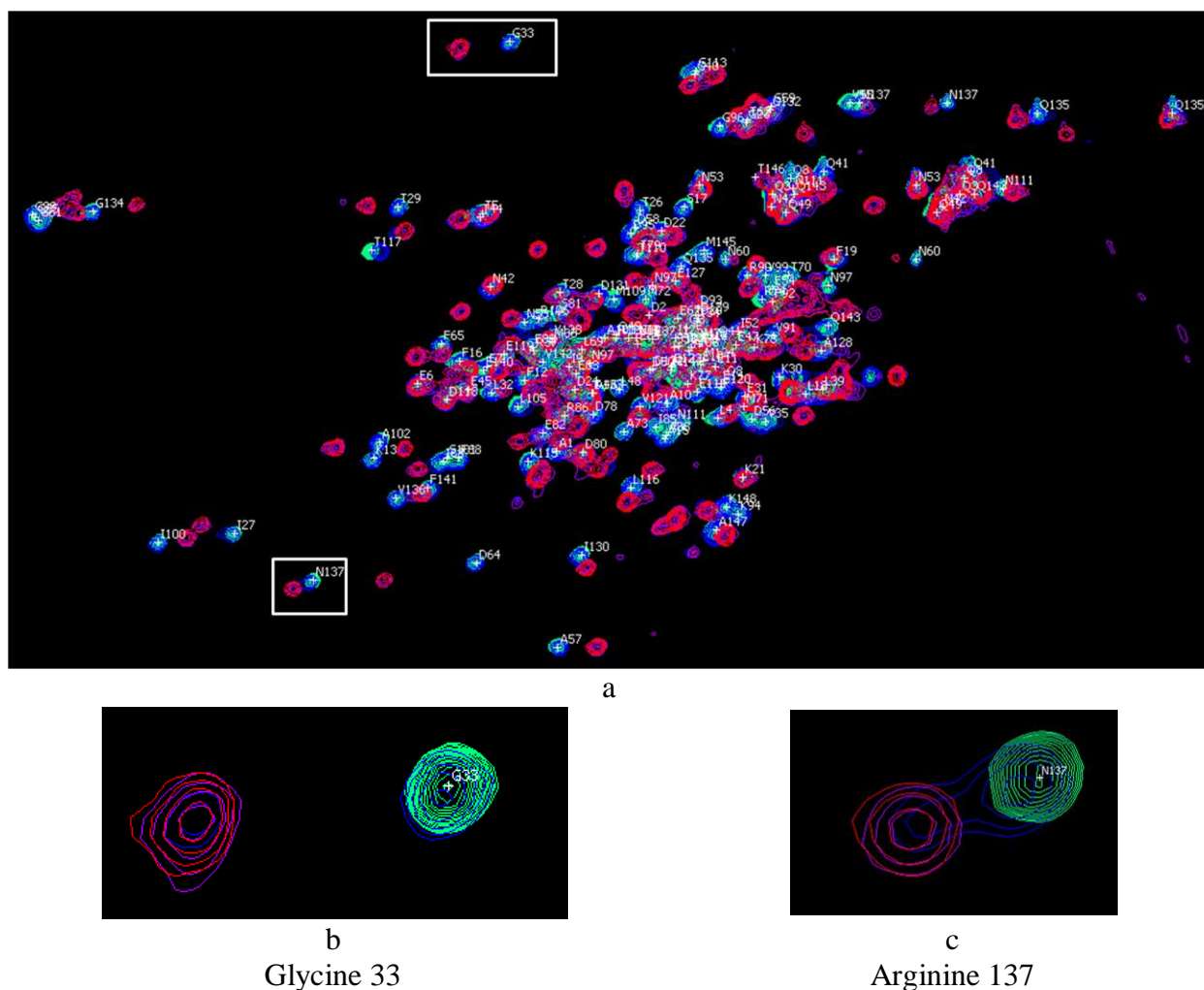
Figure 2.13. Overlay of HSQC spectra of CaM being titrated with iNOS peptide
The initial HSQC spectrum of CaM (colour aqua) was overlaid with the spectrum of different ratios of iNOS peptide to Ca^{2+}-CaM. The ratios are 1:3 ratio (blue), 2:3 ratio (purple) and 1:1 ratio (red). (a) The HSQC spectra show amino acid residues in calmodulin with the assignments belonging to the peptide-free CaM. The two lower images (b & c), demonstrate the chemical shifts of the amino acids, G33 and N137, as the iNOS peptide saturation levels increased. Spectra produced from Bruker 600 spectrophotometer and image was made using CARA, version 1.8.4.

During the titration process of Ca^{2+}-CaM with iNOS peptide, two distinct peaks corresponding to the free Ca^{2+}-CaM and peptide bound Ca^{2+}-CaM were observed such as in Figure 2.13b and c. As more peptide was added, the free CaM peak became weaker and the peak

of the bound CaM was stronger. This pattern indicates a slow exchange regime between the two states and therefore the interaction between the iNOS peptide and CaM is tight binding (Reid, 1997).

For the backbone assignment, the strategy in section 2.2.5.3 was used where each peak in the saturated CaM HSQC spectrum was assigned a peak number. An additional method was used in conjunction with the previous method since CaM contains more amino acid residues than the iNOS peptide. The NMR peak list of free holo-CaM is available on the Biological Magnetic Resonance Bank (BMRB) website as BMRB 6541 and was used to assign the peptide free holo-CaM. Using the results from the HSQC from the iNOS peptide titration (Figure 2.13), some amino acid residues were assigned and used as assigning starting points. The majority of these starting points were of amino acids outside the cluster of peaks located in the middle of the spectrum where some ambiguities can arise. In most cases peaks in the cluster could be assigned if they lined up well in the *StripScope* function (Figure 2.14), where D20 and D24 are located in the cluster.
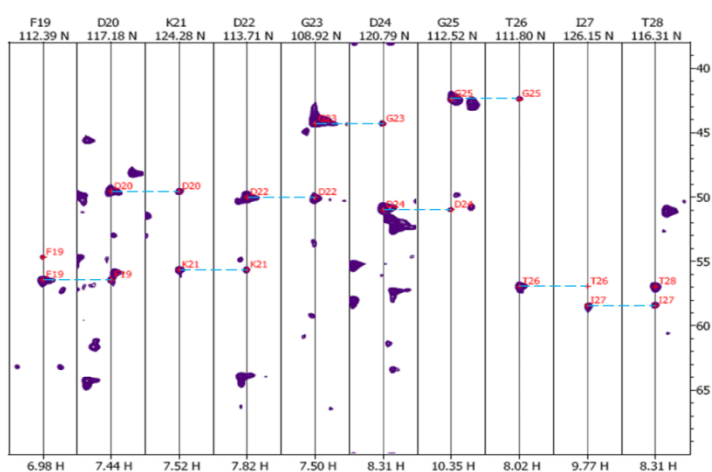
Figure 2.14. The amino acid fragment, phenylalanine 19 to theronine 28, of CaM alpha carbon alignment and overlapping using the HNCA spectrum in StripScope view.
Each strip presented is at a specific nitrogen and proton correlations plane and the peaks presented are alpha carbon peaks of the amino acid (larger peak) and the preceding alpha carbon (smaller peak).

Currently about 60% of the backbone assignments have been completed (Appendix D). The main area of assignments is in the EF hand regions whereas the central linker region has yet to be accurately assigned. In Figure 2.15, the highlighted regions are the areas that have been assigned.
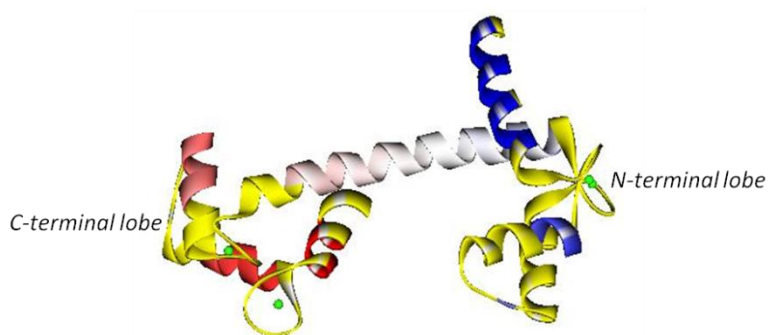
Figure 2.15. Crystal structure of CaM showing residues with NMR assignments.
The yellow highlighted areas are the amino acids that have their backbone (H, N, C_α and C_β) assigned to the NMR data. The EF hand regions are located near the four Ca^{2+} ions (green sphere). The centre linker region, the large α-helix, joining the N-terminal lobe (blue) to the C-terminal lobe (red), has yet to be assigned.

Based on the current backbone assignments, a comparison of CaM chemical shifts in its unbound form and its peptide bound form (Figure 2.16) shows a slightly larger change in the N-terminal lobe of CaM than the C-terminal lobe. The greatest changes in overall chemical shifts are MET36, ILE63 and ARG106. These amino acids belong to the region just after an EF hand loop where Ca^{2+} binds. The central linker region has not been assigned, but based on the failed attempt to locate the movement of their peaks using the titration spectra it can be assumed that they would have a large change in their chemical shift.
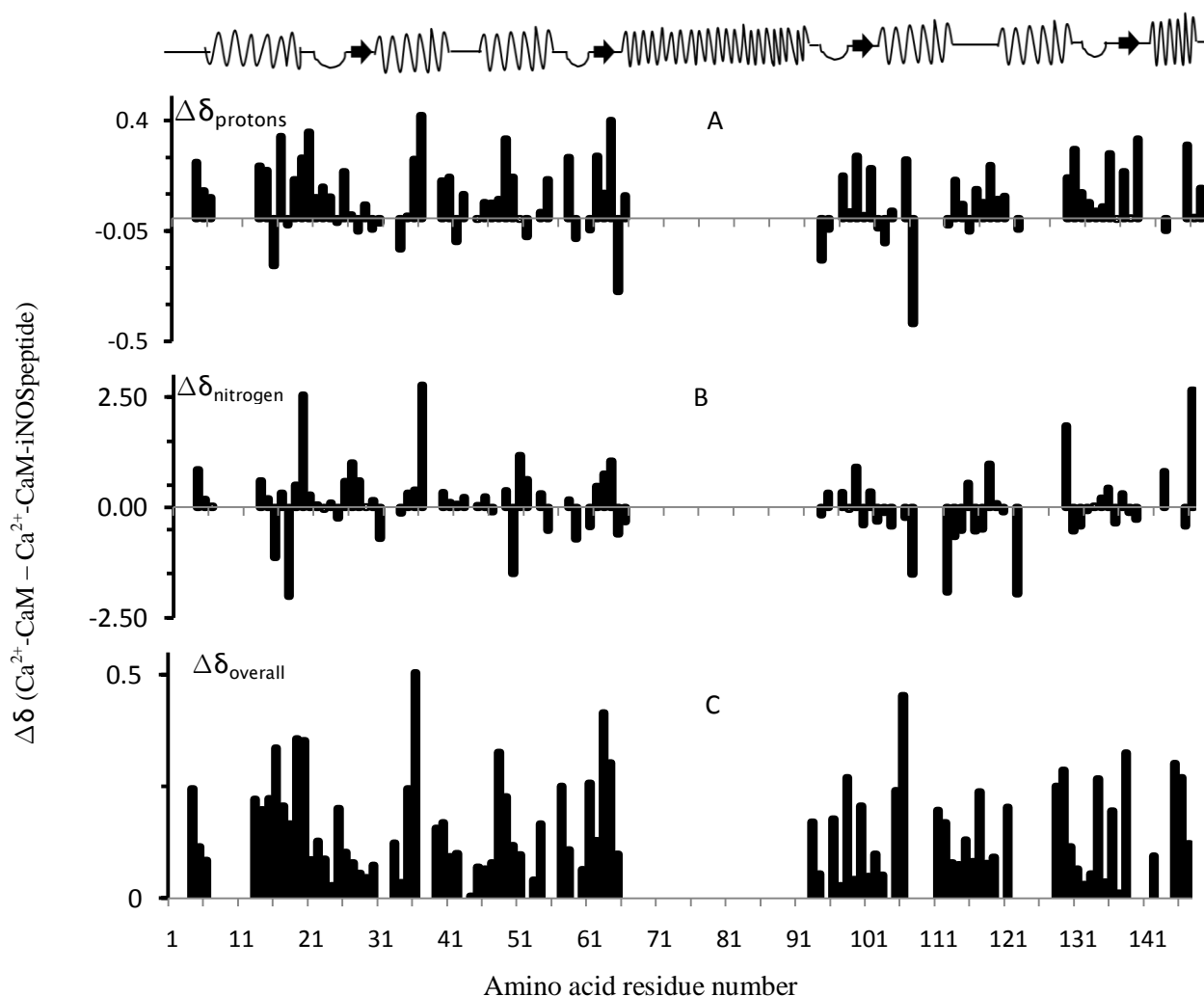
Figure 2.16. Differences in free Ca²⁺-CaM and iNOS peptide bound Ca²⁺-CaM amide chemical shifts.

The proton and nitrogen chemical shift of amides belonging to amino acid residues of Ca²⁺-CaM bound to iNOS peptide whose backbone have been assigned are compared to the chemical shift of unbound Ca²⁺-CaM. (A) The differences between the proton, (B) nitrogen and (C) overall differences. The equation $\Delta\delta_{overall} = \sqrt{(\Delta\delta H)^2 + (\Delta\delta N \cdot \frac{\gamma_N}{\gamma_H})^2}$ (Cui et al., 2003) was used to calculate the overall differences in chemical shift. The secondary structure above the graphs shows the location of residue number (undulations are helix, straight lines are random coil and the arrows are beta sheets).

2.4 Discussion

In nature iNOS is always found bound to CaM and the *in vitro* production of recombinant holo iNOS requires CaM to be co-expressed, indicating iNOS requires CaM for activation as well as stability. Even though the iNOS CaM-binding region is just two percent of the whole protein and technically twenty-four amino acids long, the extremely hydrophobic properties make it unstable in solution resulting in aggregation. The attempt to refold the intein-iNOS peptide in the inclusion bodies resulted in a lack of intein cleavage, which most likely was due to the incorrect refolding of the intein portion. The best method obtained in this investigation was the expression with the CBD-intein fusion tag and with a low induction temperature of 15°C for a period of 22 hours. The fusion tag being 55 kDa in size allows for monitoring of protein expression and provides an easy method of purification. At lower temperatures, hydrophobic interactions are reduced and protein production rates decrease. These properties increases the probability of polypeptides forming proper secondary structure without interacting with their misfolded neighbours (Vaillancourt, 2003). The induction period was increased from the original six hours to twenty hours due to better levels of expression and yields of soluble protein. Reducing the induction temperature to 15°C shocks the *E. coli* cells and the rate of translation decreases therefore a longer induction period is required for production of proteins (Vaillancourt, 2003).

CaM and the iNOS CaM-binding region peptide could not be co-expressed since there's no method of selective isotope labeling when two proteins share the same growth medium. Eventually the addition of CaM would be required since we wanted the structure of the iNOS peptide when bound to CaM. The addition of CaM during the lysis step resulted in higher yields of soluble iNOS peptide since the iNOS peptide portion of the recombinant protein will bind to

CaM and reduce the amount of free peptides available for aggregation. The addition of CaM also facilitated iNOS peptide detection after the fusion tag was cleaved off. The final yield from a 4 L culture grown in minimal media was 500 µL of 1.2 mM of purified protein.

The assignment of the NMR peaks for the iNOS CaM-binding region was much easier than that of the CaM since there is a significantly smaller number of amino acids to assign and less overlap of the peaks. The final structure was not obtained but the majority of the iNOS residues have their amino acid backbone assigned. Some analysis from the NOESY spectrum shows peak correlation between alpha protons of amino acid 'i', and the N-H of amino acid 'i+1', 'i+2' and possible 'i+3' which is a pattern characteristic of α-helices (Roberts, 1993a, Wüthrich, 1986). Since the TOCSY spectrum has yet to be run, the peaks of the amino acid side chain cannot confidently be distinguish from those peaks of adjacent amino acids or those within 5 Å.

The assignment of the NMR peaks for CaM has proven to be challenging especially in the region with large clusters of overlapping peaks in the HSQC and the amino acids in the central linker region. For the cluster and the centre linker region, there have been no easy start points that could be derived from the CaM titration spectra that did not end in false assumptions or lack of verification from the 3D spectra. The amino acid backbones of the EF hands were assigned with confidence, since the EF hands have a conserved amino acid pattern that contains glycines alternating with asparagines. Verification of sequential amino acids was simplified due to the lack of a beta carbon peak in glycine seen in the CBCAcoNH spectrum. The assignment of the EF region can provide some information on the behavior of the N-terminal and C-terminal lobes of CaM. The larger chemical shift changes in the N-terminal lobe indicate it is affected more by the binding of the iNOS peptide and therefore it could be concluded that it interacts

more readily with the iNOS peptide (Cui et al., 2003). The binding affinity of iNOS to CaM is classified as tight-binding with dissociation constant of 1.5 nM (Venema et al., 1996) which is supported by the data from the HSQC titration that show slow-exchange between peaks of free CaM and bound CaM.

During this study a crystal structure of the human iNOS FMN domain intact with the CaM-binding region (FMN-CaM binding region) was solved with a resolution of 2.5 Å (Xia et al., 2009). In one crystal, they were able to determine four different conformations of the FMN-CaM binding region bound to CaM with the aid of known structure of the FMN domain from nNOS reductase domain (Garcin et al., 2004). Using the crystallography software *Phaser* and some model rebuilding and adjustment, they were able to locate and compose the four different conformations of the FMN-CaM binding region with CaM bound (Figure 2.17 a-d).
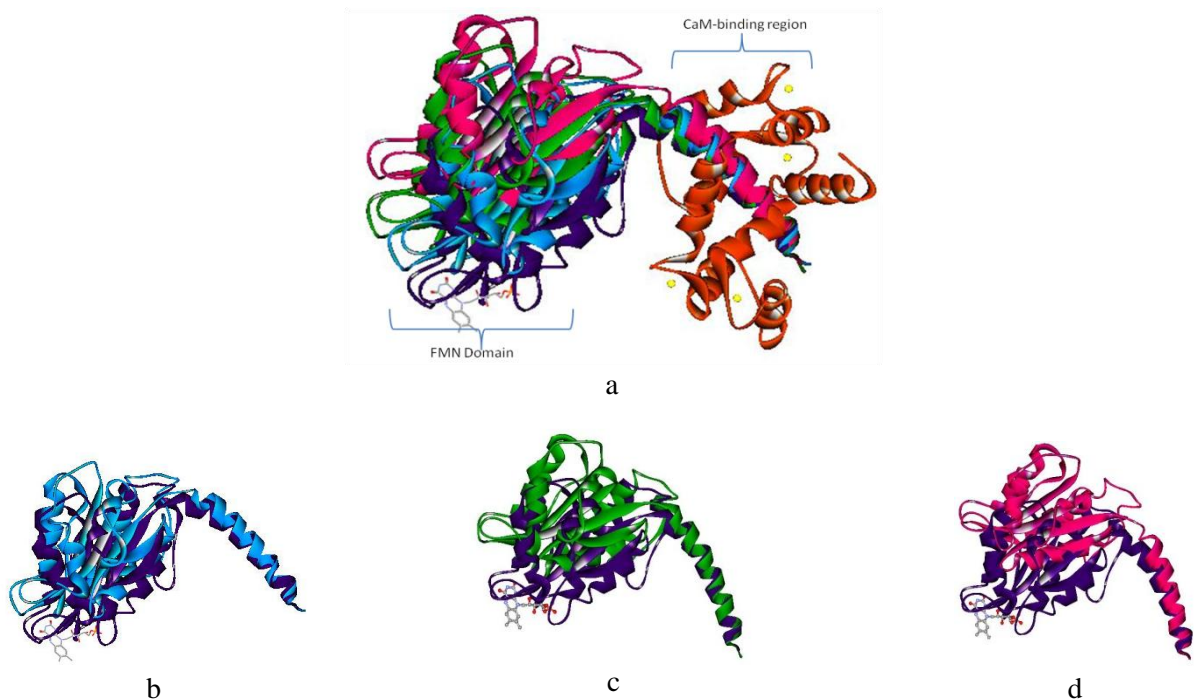
Figure 2.17.Crystal structures of the iNOS FMN domain and the CaM binding region with CaM bound to it.
The four structures solved by Xia, et al. (2009) were superimposed by aligning the CaM binding domain to show the range of motion of the FMN domain. (a) Shows all four structures superimposed with Ca^{2+}(yellow sphere)-bound CaM (orange) wrapped around the CaM-binding region. (b)-(d) Compares the movement of each structure with respect to the purple structure with the bound CaM removed. (b) has the least amount of movement and (d) the largest. The FMN cofactor of the purple structure is shown as ball and stick figure. Structures were made from PDB 3HR4 using Accelrys DS visualize 2.5.

It can be seen that the FMN domain does move towards the expected position of the heme donor. In Figure 2.17d, the distance change of the two structures (purple and pink) was measured to be 22 Å when using residue Asp595, which is located near the FMN cofactor. If the large FMN shift was proposed to be a 55 Å shift by Garcin et al. (2004), then this 22 Å difference shows that the FMN domain is dynamic but it only shows half of the possible movement. However, an important flexible hinge region was found located at Arg536 at the end of the CaM-binding region. This amino acid is fully conserved in all three isoforms and is proposed to be involved in the movement of the FMN domain (Xia et al., 2009).

The CaM bound to this crystal structure exhibited relatively similar conformation with crystal structures of the other isoforms (Figure 2.18). The iNOS peptide was found to bind in an antiparallel manner as was predicted by Spratt et al. (2007b) and forms an α-helix, which confirms some of the NOE in the NOESY spectrum (Figure 2.11). The reported crystal structures show that there are some major differences that contribute to the tight binding between the iNOS peptide and CaM. The N-terminal lobe of CaM binds at a closer proximity to the iNOS peptide than the other isoforms (Figure 2.18) which could explain the larger change in chemical shift of the N-terminal lobe seen in our NMR data (Figure 2.16). The largest change was found for Met36 and Ile63 in the N-terminal lobe and the amino acids that they interact with on the C-terminus of the iNOS peptide are shown in Figure 2.19. Met36 and Ile63 interact with key hydrophobic amino acids in the iNOS peptide such as Leu528 which is one of the anchoring amino acid residues. Flanking each side of Leu528 are Met residues that add in the tighter binding to the N-terminal lobe of CaM. Arg106 also showed a large change in chemical shift but examining the location of this residue indicated no interaction with amino acid on the iNOS peptide. Instead it points away from the cavity of the iNOS peptide towards the solvent.
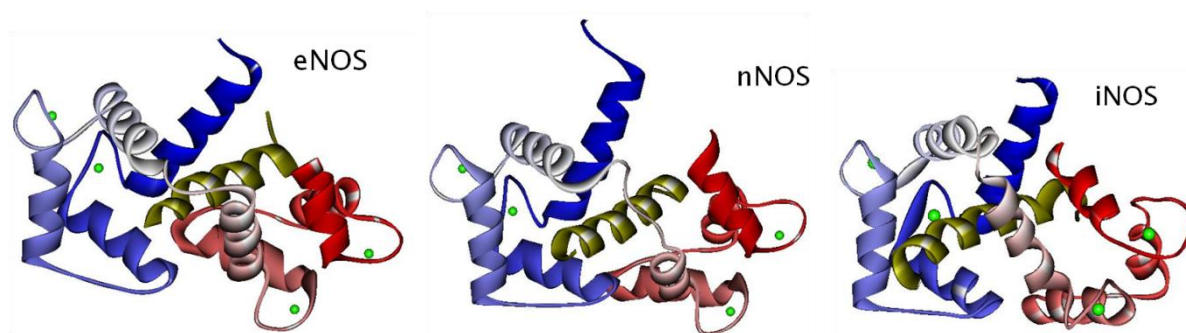
Figure 2.18. Crystal structure of eNOS, nNOS and iNOS CaM-binding region bound to CaM
Comparison of the CaM binding region of the three isoforms (gold) in complex with CaM (blue and red which represent N- and C-terminal lobes, respectively). The cNOS enzymes are very similar whereas iNOS has CaM more tightly wrapped especially in the N-terminal. The centre linker region is also not as extended as the other isoforms. Figure made from 1NIW, 2O60 and 3HR4 for nNOS, eNOS and iNOS, respectively using Accelrys DS visualize 2.5.
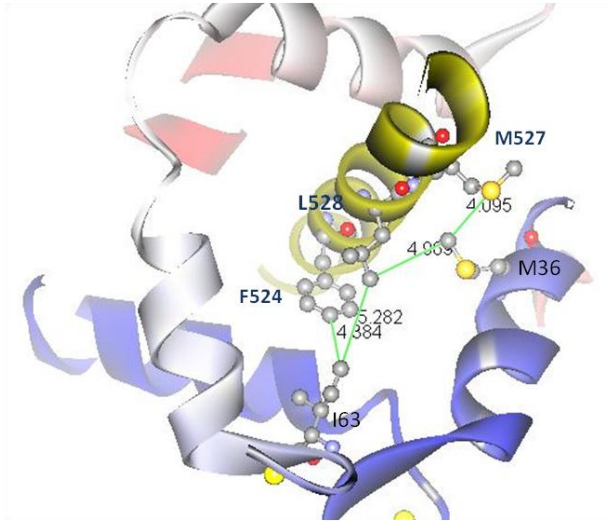
Figure 2.19. Met36 and Ile63 of CaM interacting with the C-terminal of the iNOS peptide. Methionine 36 and isoleucine 63 are shown as ball and stick figure branching from the blue ribbon structure of the N-terminal lobe of CaM. The amino acids that they interact with are indicated by green lines connecting the two residues. Met36 interacts with Met527 (4.095 Å) and Leu528 (4.969 Å) on the iNOS peptide whereas Leu63 interacts with Leu528 (5.282 Å) and Phe524 (4.384 Å) through hydrophobic interactions. Figure made from PDB 3HR4 (Xia et al., 2009) using Accelrys DS visualize 2.5.

The structure of the iNOS FMN domain with the CaM binding region is the first structural evidence of movement in the FMN domain. Xia et al (2009) went further and superimposed the FMN of the iNOS onto the FMN site of the existing crystal structure of nNOS reductase domain to create a model for electron transfer from the FAD to the heme. Based on this model, they were able to determine that the FAD, FMN and the CaM have very little contact during the electron transfer. This point indicates the three partitions are flexing away from each other and that there must also be another hinge region connecting the CaM binding domain and the heme region (Xia et al., 2009). When the oxygenase domain and the dimer were accounted for in the model, the FMN domain interface had the most contacts with the oxygenase domain of the opposite monomer.

60

The new published structure shows some of the dynamic properties of the FMN domain and an insight into factors contributing to the tight binding of CaM to iNOS. The results obtained so far from our NMR investigation of iNOS CaM-binding region have been supported by this crystal structure particularly in the CaM-binding region. As the assignments of the NMR spectra continue, this structure will be used as for comparison.

Chapter 3 Future Work

Once the backbone or full assignments of CaM have been completed, another aspect that can be examined is the effect that posttranslational modification of calmodulin has on the interactions with the NOS CaM-binding region. Calmodulin *in vivo* can be regulated in many ways such as phosphorylation, oxidation and by interaction with small peptides (Benaim and Villalobo, 2002). These modes of regulation can alter CaM's structure and methods of interaction with target proteins that may result in inhibiting the binding of CaM or reducing enzyme function (Benaim and Villalobo, 2002). Mode of regulation of interest is phosphorylation which occurs at specific tyrosine residues on CaM. To study phosphorylation of these sites, selected tyrosine residues were mutated to aspartic acid or glutamic acid, which mimicked the electrostatics properties of phosphorylated residues (Spratt et al., 2008). Kinetic assay studies in our lab have found that tyrosine 99 mutated to aspartic acid had a significant reduction in enzymatic activity (Israel, 2010). Therefore examining the effects of T99Y on the structure of CaM and how it interacts with the iNOS peptide using NMR spectroscopy will show what is occurring on the structural level. The full backbone assignment of wild-type CaM bound to the iNOS CaM-binding region in the HSQC spectrum can be compared to the HSQC of the mutant CaM. Factors to look for are peak shifts of the mutated amino acid(s) in adjacent amino acids and in the immediate area.

Another side project is the NMR experiments which have been acquired for CaM interaction with iNOS CaM binding domain, which have been shared with Ming Li, a researcher in the UW Math department whose group is currently writing a program to automatically assign NMR spectra of CaM. Collaboration with one of Dr. Li's students, Richard Yang, has required analyzing and comparing their chemical shifts to the ones that have been assigned thus far.

Future work with this group will aid in faster assignments of mutant CaMs and CaM bound to other NOS isoforms.

The dynamics of the FMN domain and further characterization of the effects induced by CaM can be done using NMR spectroscopy. NMR spectroscopy can provide a family of best fit structures that can show the range of movement using spin relaxation experiments to determine changes in chemical shift and the exchange rate in a period of time (Wüthrich, 1986). The methods used in the solved structure of the FMN domain by (Xia et al., 2009), can also aid in providing expression and purification conditions to produce soluble proteins required for these NMR experiments.

Appendix A – Mass Spectrometer result of CaM bound to iNOS CaM-binding region

The 3391 Da peak corresponds to the iNOS peptide.
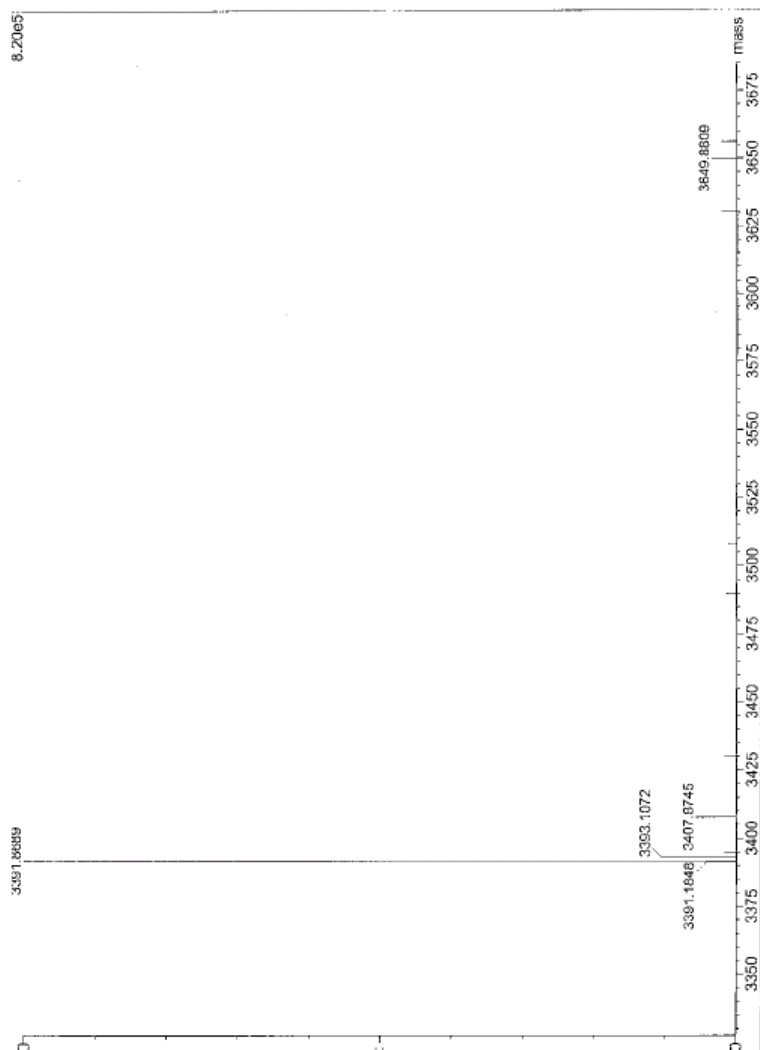
The 16704 kDa peak corresponds to CaM.
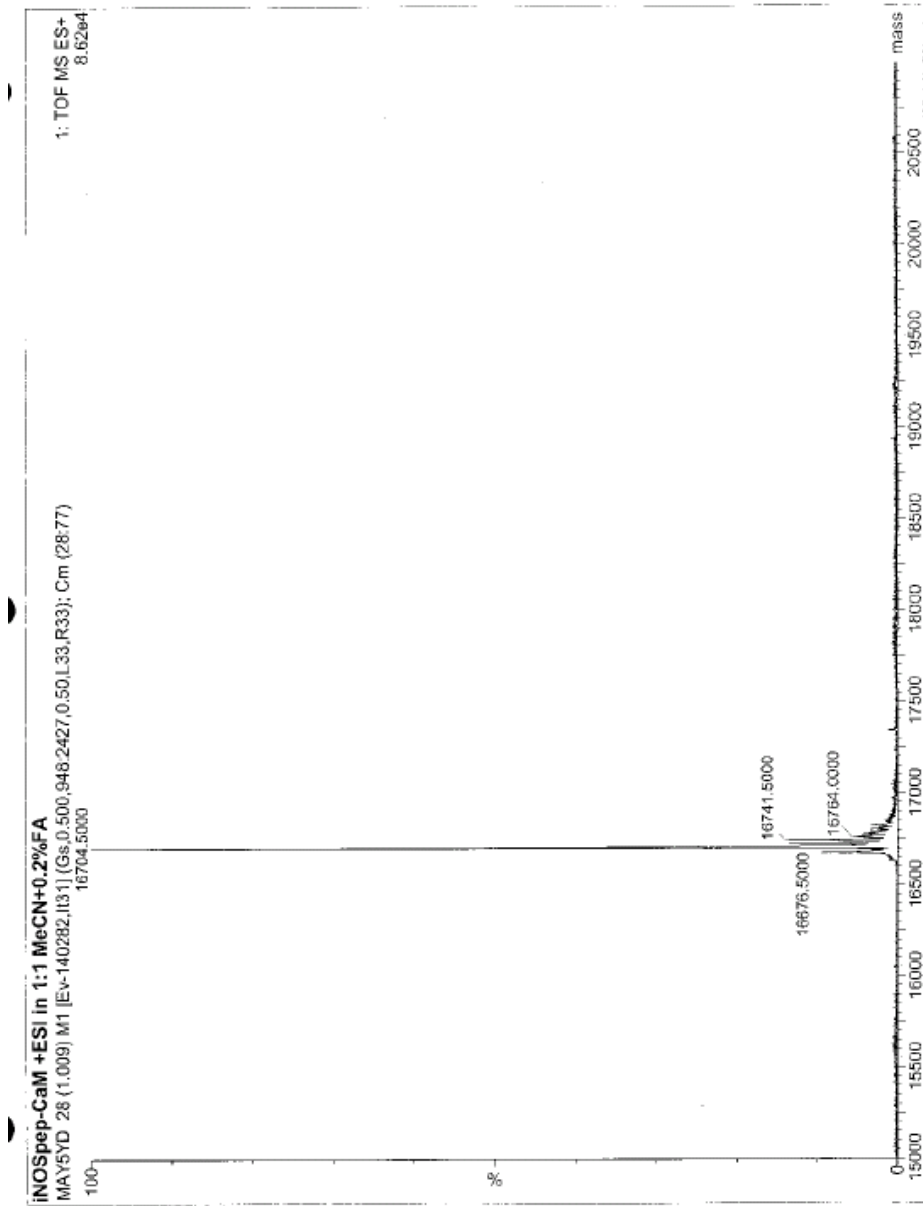
Appendix B – NMR file location and pulse sequence

Spectrum Name	Isotope labeled	Spectrum Type	D	Folder location
wtCaM-iNOSpep 13C-NOESY HSQC	C, N	3D C13ali-NOESY	3	CN_WT_Cal_iNOS/7/pdata/1/3rr
wtCaM-iNOSpep 15N-HSQCb4 15N-NOESY	C, N	Hsqc15N	2	CN_WT_Cal_iNOS/3/pdata/1/2rr
wtCaM-iNOSpep 15N-HSQCb4 CBCAcoNH	C, N	Hsqc 15N	2	CN_WT_Cal_iNOS/1/pdata/1/2rr
wtCaM-iNOSpep 15N-HSQCb4 HCH-TOCSY	C, N	Hsqc 15N	2	CN_WT_Cal_iNOS/5/pdata/1/2rr
wtCaM-iNOSpep 15N-HSQC titration 1	C, N	Hsqc 15N	2	CAM_CN_iNOS_700/1/pdata/1/2rr
wtCaM-iNOSpep 15N-HSQC titration 2	C, N	Hsqc 15N	2	CAM_CN_iNOS_700/2/pdata/1/2rr
wtCaM-iNOSpep 15N-HSQC titration 3	C, N	Hsqc 15N	2	CAM_CN_iNOS_700/3/ pdata/1/2rr
wtCaM-iNOSpep 15N-HSQC titration 4**	C, N	Hsqc 15N	2	CAM_CN_iNOS_700/4/ pdata/1/2rr
wtCaM-iNOSpep 15N-NOESY HSQC	C, N	3D N15-NOESY	3	CN_WT_Cal_iNOS/4/pdata/1/3rr
wtCaM-iNOSpep CBCAcoNH	C, N	CBCAcoNH	3	CN_WT_Cal_iNOS/2/pdata/1/3rr
wtCaM-iNOSpep HCCH-TOCSY	C, N	HCcH-TOCSYali	3	CN_WT_Cal_iNOS/6/pdata/1/3rr
wtCaM-iNOSpep HNCA	C, N	HNCA	3	CAM_CN_iNOS_700/6/pdata/1/3rr
wtCaM-iNOSpep HNCOCA	C, N	HN(CO)CA	3	CAM_CN_iNOS_700/7/pdata/1/3rr
wtCAM HSQC	N	Hsqc 15N	2	Calmodulin Spectra/CAM_15N/13C/1/pdata/1/2rr
wtCaM-iNOSpep HSQC ref spectrum***	N	Hsqc 15N	2	NMR 600 – Data/CAM_iNOS_15N/1/pdata/1/2rr
wtCaM-iNOSpep NOESY	N	3D N15-NOESY	3	NMR 600 – Data/CaM_iNOS_15N/2/pdata/1/3rr
wtCaM-iNOSpep TOCSY	N	3D N15-TOCSY	3	NMR 600 – Data/CaM_iNOS_15N/3/pdata/1/3rr
iNOSpeptile NOESY	C, N	3D NOESY	3	iNOS_13C_09_3_pdata_1
iNOSpeptile 15N-HSQC	C, N	2D HSQC	2	iNOS_13C_CAM/1/pdata/1/2rr
iNOSpeptile HNCA	C, N	HNCA	3	iNOS_13C_CAM/2/pdata/1/3rr
iNOSpeptile NOSEY	C, N	NOESY	3	iNOS_13C_CAM/3/pdata/1/3rr
15N wtCaM HSQC – no iNOSpep	C, N	Hsqc 15N	2	CAM_CN_iNOS_700/1/pdata/1/2rr
15N wtCaM-iNOSpep HSQC – titration 1	C, N	Hsqc 15N	2	CAM_CN_iNOS_700/2/pdata/1/2rr

HSQC:

```
# 1 "/opt/xwinnmr/exp/stan/nmr/lists/pp/hsqcetf3gpsi"
;hsqcetf3gpsi
;avance-version (02/07/15)
;HSQC
;2D H-1/X correlation via double inept transfer
;   using sensitivity improvement
;phase sensitive using Echo/Antiecho-TPPI gradient selection
;with decoupling during acquisition
;using trim pulses in inept transfer
;using f3 - channel
;
;A.G. Palmer III, J. Cavanagh, P.E. Wright & M. Rance, J. Magn.
;   Reson. 93, 151-170 (1991)
;L.E. Kay, P. Keifer & T. Saarinen, J. Am. Chem. Soc. 114,
;   10663-5 (1992)
;J. Schleucher, M. Schwendinger, M. Sattler, P. Schmidt, O. Schedletzky,
;   S.J. Glaser, O.W. Sorensen & C. Griesinger, J. Biomol. NMR 4,
;   301-306 (1994)
```

HNCA:

```
# 1 "/opt/xwinnmr/exp/stan/nmr/lists/pp/hncagp3d"
;hncagp3d
;avance-version (02/05/31)
;HNCA
;3D sequence with
;   inverse correlation for triple resonance using multiple
;      inept transfer steps
;
;      F1(H) -> F3(N) -> F2(Ca,t1) -> F3(N,t2) -> F1(H,t3)
;
;on/off resonance Ca and C=O pulses using shaped pulse
;phase sensitive (t1)
;phase sensitive using Echo/Antiecho gradient selection (t2)
;using constant time in t2
```

```
;(use parameterset HNCAGP3D)
;
;S. Grzesiek & A. Bax, J. Magn. Reson. 96, 432 - 440 (1992)
;(J. Schleucher, M. Sattler & C. Griesinger, Angew. Chem. Int. Ed. 32,
;  1489-1491 (1993))
;(L.E. Kay, G.Y. Xu & T. Yamazaki, J. Magn. Reson. A109, 129-133 (1994))

prosol relations=<triple>
```

HNcoCA:

```
# 1 "/opt/xwinnmr/exp/stan/nmr/lists/pp/hncocagp3d"
;hncocagp3d
;avance-version (03/08/05)
;HN(CO)CA
;3D sequence with
;   inverse correlation for triple resonance using multiple
;      inept transfer steps
;
;      F1(H) -> F3(N) -> F2(C=O) -> F2(Ca,t1)
;              -> F2(C=O) -> F3(N,t2) -> F1(H,t3)
;
;on/off resonance Ca and C=O pulses using shaped pulse
;phase sensitive (t1)
;phase sensitive using Echo/Antiecho gradient selection (t2)
;using constant time in t2
;(use parameterset HNCOCAGP3D)
;
;S. Grzesiek & A. Bax, J. Magn. Reson. 96, 432 - 440 (1992)
;(L.E. Kay, G.Y. Xu & T. Yamazaki, J. Magn. Reson. A109, 129-133 (1994))

prosol relations=<triple>
```

CBCAcoNH:

```
# 1 "C:/Bruker/XWIN-NMR/exp/stan/nmr/lists/pp/cbcaconhgpwg3d"
;cbcaconhgpwg3d
;avance-version (02/05/31)
;CBCACONH
;3D sequence with
;   inverse correlation for triple resonance using inept transfer steps
;
;      F1(H) -> F2(Caliph.,t1 -> Ca) -> F2(C=O) -> F3(N,t2) -> F1(H,t3)
;
;on/off resonance Ca and C=O pulses using shaped pulse
;phase sensitive (t1)
;phase sensitive (t2)
;using constant time in t1
;using constant time in t2
;water suppression using watergate sequence
;(use parameterset CBCACONHGPWG3D)
;
;S. Grzesiek & A. Bax, J. Biomol. NMR 3, 185-204 (1993)
;(D.R. Muhandiram & L.E. Kay, J. Magn. Reson. B 103, 203-216 (1994))

prosol relations=<triple>
```

15N-HSQC (2D):

```
# 1 "C:/Bruker/XWIN-NMR/exp/stan/nmr/lists/pp/invifpf3gpsid31"
;invifpf3gpsi
;avance-version
;2D H-1/X correlation via double inept transfer
;   using sensitivity improvement
```

```
;phase sensitive using Echo/Antiecho-TPPI gradient selection
;with decoupling during acquisition
;using f3 - channel
;using flip-back pulse
;A.G. Palmer III, J. Cavanagh, P.E. Wright & M. Rance, J. Magn.
;   Reson. 93, 151-170 (1991)
;L.E. Kay, P. Keifer & T. Saarinen, J. Am. Chem. Soc. 114,
;   10663-5 (1992)
;J. Schleucher, M. Schwendinger, M. Sattler, P. Schmidt, O. Schedletzky,
;   S.J. Glaser, O.W. Sorensen & C. Griesinger, J. Biomol. NMR 4,
;   301-306 (1994)
;S. Grzesiek & A. Bax, J. Am. Chem. Soc. 115, 12593-12594 (1993)
;modified by jgaspar to include delay prior to aquisition
;
```

^{13}C-NOESY HSQC:

```
#1 "C:/Bruker/XWIN-NMR/exp/stan/nmr/lists/pp/noesyhsqcetgp3d"
;noesyhsqcetgp3d
;avance-version (02/07/15)
;NOESY-HSQC
;3D sequence with
;   homonuclear correlation via dipolar coupling
;   dipolar coupling may be due to noe or chemical exchange.
;   H-1/X correlation via double inept transfer
;      using sensitivity improvement
;phase sensitive (t1)
;phase sensitive using Echo/Antiecho-TPPI gradient selection (t2)
;using trim pulses in inept transfer
;with decoupling during acquisition
;using shaped pulses for inversion on f2 - channel
;(use parameterset NOESYHSQCETGP3D)
;
;A.L. Davis, J. Keeler, E.D. Laue & D. Moskau, J. Magn. Reson. 98,
;   207-216 (1992)
;A.G. Palmer III, J. Cavanagh, P.E. Wright & M. Rance, J. Magn.
;   Reson. 93, 151-170 (1991)
;L.E. Kay, P. Keifer & T. Saarinen, J. Am. Chem. Soc. 114,
;   10663-5 (1992)
;J. Schleucher et al., Angew. Chem. 114(10), 1518 (1993)
```

^{15}N-NOESY HSQC:

```
# 1 "C:/Bruker/XWIN-NMR/exp/stan/nmr/lists/pp/noesyhsqcfpf3gpsi3d"
;noesyhsqcfpf3gpsi3d
;avance-version (03/06/18)
;NOESY-HSQC
;3D sequence with
;   homonuclear correlation via dipolar coupling
;   dipolar coupling may be due to noe or chemical exchange
;   H-1/X correlation via double inept transfer
;      using sensitivity improvement
;phase sensitive (t1)
;phase sensitive using Echo/Antiecho-TPPI gradient selection (t2)
;with decoupling during acquisition
;using flip-back pulse
;using f3 - channel
;(use parameterset NOESYHSQCFPF3GPSI3D)
;
;O. Zhang, L.E. Kay, J.P. Olivier & J.D. Forman-Kay,
;   J. Biomol. NMR 4, 845 - 858 (1994)
;A.G. Palmer III, J. Cavanagh, P.E. Wright & M. Rance, J. Magn.
;   Reson. 93, 151-170 (1991)
;L.E. Kay, P. Keifer & T. Saarinen, J. Am. Chem. Soc. 114,
;   10663-5 (1992)
;J. Schleucher, M. Schwendinger, M. Sattler, P. Schmidt, O. Schedletzky,
;   S.J. Glaser, O.W. Sorensen & C. Griesinger, J. Biomol. NMR 4,
```

```
;    301-306 (1994)

prosol relations=<triple>
```

HCCH-TOCSY:

```
# 1 "C:/Bruker/XWIN-NMR/exp/stan/nmr/lists/pp/hcchdigp3d"
;hcchdigp3d
;avance-version (03/01/17)
;HCCH-TOCSY
;3D sequence with
;    inverse correlation using multiple inept transfer and
;       C-C DIPSI3 spinlock
;
;       F1(H,t1) -> F2(C,t2) -> F2(C') -> F1(H',t3)
;
;off resonance C=O pulse using shaped pulse
;phase sensitive (t1)
;phase sensitive (t2)
;spinlock during z-filter
;(use parameterset HCCHDIGP3D)
;
;(L.E. Kay, G.Y. Xu, A.U. Singer, D.R. Muhandiram & J. D. Forman-Kay
;    J. Magn. Reson. B 101, 333 - 337 (1993))


prosol relations=<triple>
```

Appendix C – iNOS Peptide Assigned Chemical shift

Peak #	A.a #	H_N	C_α	N
1	L 13	10.244	55.558	128.211
2	L 21	8.89	56.253	121.099
3	K 14	8.844	56.947	114.853
4	V 17	8.689	64.213	111.605
5	C 24	8.538	61.395	114.936
6	M 25	8.493	56.173	120.181
7	A 19	7.778	53.176	120.248
8		8.433	53.368	123.329
9		8.365	51.258	123.7
10		8.285	55.585	122.852
11		8.266	53.047	122.736
12		7.903	54.116	122.584
13		8.334	52.673	121.624
14		8.286	53.587	121.463
15	R 28	8.029	53.341	122.102
16		8.348	52.887	118.363
17	V 20	8.275	64.48	116.528
19	F 22	7.925	58.87	118.491
20	L 16	7.784	55.366	120.332
21	K 29	7.91	54.81	127.772
22	A 23	7.665	52.78	117.515
23		7.469	40.533	120.347
24		7.318	40.541	120.333
25	M 27	7.239	54.196	116.892
26	L 26	7.163	52.994	117.793
28	K 18	7.143	57.829	119.476
29		7.083	40.707	119.89
30	V 15	6.755	63.212	117.347
31		8.054	50.85	121.067
32		8.233	55.31	128.349

Appendix D - CaM assigned chemical shift

Peak #	A.a #	H_N	C_α	N	Peak #	A.a #	H_N	C_α	N
1	G 25	10.354	42.401	112.516	48	M 145	7.47	53.319	114.939
2	G 98	10.299	42.106	112.074	49	Y 99	7.496	53.669	116.012
3	G 134	10.039	42.938	112.38	50		7.556	58.947	114.722
4	G 33	8.694	45.654	105.632	51	G 113	7.742	42.411	107.29
5	G 61	7.48	42.697	108.13	52	G 40	7.636	42.631	106.794
6	T 29	9.079	63.992	112.495	53	G 96	7.528	44.156	108.825
7	T 117	8.93	57.95	113.529	54	G 23	7.502	44.296	108.925
8	T 44	8.693	57.929	113.057	55	T 62	7.48	56.884	108.13
9	T 5	8.574	57.674	112.776	56		7.467	44.526	108.306
10	I 100	9.831	58.597	126.813	56	G 132	7.458	44.352	108.423
11	I 27	9.768	58.432	126.149	58	F 19	6.977	56.428	112.386
12	N 137	9.387	48.084	128.895	59		7.15	58.947	114.62
13	D 64	9.006	49.289	128.6	60	A 57	8.124	51.183	131.498
14	A 102	9.209	53.063	122.898	61	I 130	8.168	60.568	128.09
15	K 13	8.925	57.151	122.912	62	L 116	8.002	51.402	125.255
16	E 6	8.873	57.748	120.252	63	K 148	7.803	54.764	126.002
17	R 106	8.882	57.436	118.96	64	K 94	7.67	55.728	125.575
18	S 101	8.87	53.177	123.812	65	A 147	7.594	50.088	126.583
19	V 136	8.855	58.684	124.898	66	K 21	7.52	55.64	124.285
20	F 65	8.764	60.166	118.898	67	N 111	7.907	52.924	123.876
21	D 118	8.756	55.18	120.864	68	A 15	8.117	52.76	123.8
22	E 45	8.68	57.315	120.304	69	V 121	8.072	58.443	123.213
23		8.715	55.503	120.047	70		8.191	51.731	123.212
24		8.664	56.1	119.522	70	L 4	7.481	51.717	120.921
25		7.575	57.191	121.362	71	K 115	8.378	52.903	124.176
25		8.537	57.191	119.657	72	I 63	8.447	57.819	122.6
26		8.517	51.939	120.428	73		7.695	52.669	118.387
27	E 119	8.504	57.13	119.095	73		8.282	52.669	122.572
28	V 142	8.484	64.225	118.546	74		8.208	56.841	121.987
29	F 16	8.445	58.991	118.968	75	L 105	8.301	55.662	121.476
30		8.421	59.509	119.249	76	D 24	8.314	50.988	120.787
31		8.691	63.896	117.008	77		8.413	51.917	120.251
32	N 42	8.558	48.61	115.871	78		8.321	51.797	119.97
33	M 36	7.975	55.157	115.68	79		8.241	55.334	120.05
33	N 53	8.485	56.585	117.299	80		8.196	52.673	119.803
34		8.378	61.378	114.327	81		8.222	51.698	120.783
35	T 28	8.306	56.943	116.306	81	L 39	7.121	54.745	120.228
36		8.282	56.833	122.572	82	D 133	8.182	50.822	120.481
36		8.331	56.833	118.259	83	A 46	8.16	52.298	120.793
37		8.196	52.979	117.391	84		7.952	52.662	121.545
38	D 131	8.14	51.36	116.474	85	A 103	8.151	52.465	118.719
39	D 58	8.129	49.946	114.225	86	N 60	8.094	49.88	118.727
40	T 26	8.015	56.932	111.799	87	D 50	7.991	56.867	118.54
41		7.94	50.231	113.981	88		7.924	57.502	118.514
42	D 22	7.816	50.034	113.714	89	M 51	7.891	56.724	118.106
43	S 17	7.875	58.969	114.684	90		7.977	54.688	117.142
45	Q 135	7.865	50.472	115.578	91	D 93	7.957	49.837	117.212
46		7.786	57.94	115.757	92		7.842	56.297	117.493
47		7.729	55.082	116.191	93	T 34	7.783	64.247	117.263

Appendix D continued-CaM assigned chemical shift

Peak #	A.a #	H$_N$	C$_\alpha$	N	Peak #	A.a #	H$_N$	C$_\alpha$	N
94	Q 41	7.806	50.844	118.284	156		8.18	57.813	120.69
95		7.695	56.702	118.387	158		7.922	51.41	125.018
96		7.67	61.159	117.544	160		7.925	54.696	113.887
97		7.701	61.663	116.906	160		7.925	63.933	113.887
98	Q 49	7.962	57.031	119.657	161		7.931	57.776	118.47
99		7.909	54.917	119.638					
100		7.896	64.137	120.48					
101	E 114	7.847	51.489	120.065					
102		7.81	56.797	119.647					
103		7.758	54.808	120.104					
104	E 14	7.499	56.439	120.078					
104	L 48	7.794	56.575	120.144					
106	E 47	7.554	56.449	118.6					
107		7.489	56.574	118.675					
108		7.421	64.214	118.683					
109	D 129	7.507	51.665	117.839					
110	D 20	7.437	49.552	117.181					
111		7.392	55.859	117					
112	E 54	7.324	55.377	116.72					
113		7.293	56.209	116.141					
114		7.261	55.979	116.463					
115	A 128	7.109	48.194	117					
116		7.325	51.424	117.94					
117		7.262	63.371	118.698					
118		7.114	56.144	119.488					
120	L 18	7.186	54.742	120.209					
121		6.882	40.2	119.817					
122		7.33	47.338	120.621					
122	K 30	7.472	56.516	120.713					
125		7.575	56.591	121.362					
126	V 35	7.27	64.334	121.515					
127		7.854	54.928	126.32					
128		8.385	57.841	122.541					
129		8.222	59.654	117.211					
130		7.724	50.603	127.424					
131	N 97	8.214	49.722	119.448					
135	Y 138	8.072	59.853	118.571					
138		8.662	54.753	119.602					
139		7.806	56.86	119.512					
140		8.154	54.741	118.825					
141		7.806	59.815	119.348					
142		7.615	52.86	119.333					
142	L 112	7.627	52.917	119.231					
145		8.379	59.085	123.754					
147		7.334	47.246	120.426					
150		7.836	51.489	120.086					
151	T 146	7.545	59.203	108.69					
153		8.188	51.745	123.092					
155		6.696	57.24	112.56					

References

Abu-Soud, H. M., Yoho, L. L. & Stuehr, D. J. (1994). Calmodulin controls neuronal nitric-oxide synthase by a dual mechanism. Activation of intra- and interdomain electron transfer. *J Biol Chem, 269,* 32047-32050.

Afshar, M., Caves, L. S., Guimard, L., Hubbard, R. E., Calas, B., Grassy, G. & Haiech, J. (1994). Investigating the high affinity and low sequence specificity of calmodulin binding to its targets. *J Mol Biol, 244,* 554-571.

Aoyagi, M., Arvai, A. S., Tainer, J. A. & Getzoff, E. D. (2003). Structural basis for endothelial nitric oxide synthase binding to calmodulin. *EMBO J, 22,* 766-775.

Babu, Y. S., Bugg, C. E. & Cook, W. J. (1988). Structure of calmodulin refined at 2.2 A resolution. *J Mol Biol, 204,* 191-204.

Barbato, G., Ikura, M., Kay, L. E., Pastor, R. W. & Bax, A. (1992). Backbone dynamics of calmodulin studied by 15N relaxation using inverse detected two-dimensional NMR spectroscopy: the central helix is flexible. *Biochemistry, 31,* 5269-5278.

Benaim, G. & Villalobo, A. (2002). Phosphorylation of calmodulin. Functional implications. *Eur J Biochem, 269,* 3619-3631.

Brändén, C.-I. & Tooze, J. (1999). *Introduction to protein structure,* (Editor ed.). New York: Garland Pub.

Craig, D. H., Chapman, S. K. & Daff, S. (2002). Calmodulin activates electron transfer through neuronal nitric-oxide synthase reductase domain by releasing an NADPH-dependent conformational lock. *J Biol Chem, 277,* 33987-33994.

Cui, Y., Wen, J., Hung Sze, K., Man, D., Lin, D., Liu, M. & Zhu, G. (2003). Interaction between calcium-free calmodulin and IQ motif of neurogranin studied by nuclear magnetic resonance spectroscopy. *Anal Biochem, 315,* 175-182.

Daff, S., Noble, M. A., Craig, D. H., Rivers, S. L., Chapman, S. K., Munro, A. W., Fujiwara, S., Rozhkova, E., Sagami, I. & Shimizu, T. (2001). Control of electron transfer in neuronal NO synthase. *Biochem Soc Trans, 29,* 147-152.

Daff, S., Sagami, I. & Shimizu, T. (1999). The 42-amino acid insert in the FMN domain of neuronal nitric-oxide synthase exerts control over Ca(2+)/calmodulin-dependent electron transfer. *J Biol Chem, 274,* 30589-30595.

Drum, C. L., Yan, S. Z., Bard, J., Shen, Y. Q., Lu, D., Soelaiman, S., Grabarek, Z., Bohm, A. & Tang, W. J. (2002). Structural basis for the activation of anthrax adenylyl cyclase exotoxin by calmodulin. *Nature, 415,* 396-402.

Duyff, R. L. (2006). *American Dietetic Association complete food and nutrition guide,* (Editor ed.). Hoboken, N.J.: John Wiley & Sons.

Fedorov, R., Ghosh, D. K. & Schlichting, I. (2003). Crystal structures of cyanide complexes of P450cam and the oxygenase domain of inducible nitric oxide synthase-structural models of the short-lived oxygen complexes. *Arch Biochem Biophys, 409,* 25-31.

Feelisch, M. & Stamler, J. S. (1996). *Methods in nitric oxide research,* (Editor ed.). Chichester ; New York: J. Wiley.

Fischmann, T. O., Hruza, A., Niu, X. D., Fossetta, J. D., Lunn, C. A., Dolphin, E., Prongay, A. J., Reichert, P., Lundell, D. J., Narula, S. K. & Weber, P. C. (1999). Structural characterization of nitric oxide synthase isoforms reveals striking active-site conservation. *Nat Struct Biol, 6,* 233-242.

Frederick, K. K., Kranz, J. K. & Wand, A. J. (2006). Characterization of the backbone and side chain dynamics of the CaM-CaMKIp complex reveals microscopic contributions to protein conformational entropy. *Biochemistry, 45,* 9841-9848.

Garcin, E. D., Bruns, C. M., Lloyd, S. J., Hosfield, D. J., Tiso, M., Gachhui, R., Stuehr, D. J., Tainer, J. A. & Getzoff, E. D. (2004). Structural basis for isozyme-specific regulation of electron transfer in nitric-oxide synthase. *J Biol Chem, 279,* 37918-37927.

Gellman, S. H. (1991). On the role of methionine residues in the sequence-independent recognition of nonpolar protein surfaces. *Biochemistry, 30,* 6633-6636.

Ghosh, D. K. & Salerno, J. C. (2003). Nitric oxide synthases: domain structure and alignment in enzyme function and control. *Front Biosci, 8,* d193-209.

Gopalakrishna, R. & Anderson, W. B. (1981). Ca^{2+}-induced hydrophobic site on calmodulin: application for purification of calmodulin by phenyl-sepharose affinity chromatography. *Biochem Biophys Res Commun, 104,* 830-836.

Griffith, O. W. & Stuehr, D. J. (1995). Nitric oxide synthases: properties and catalytic mechanism. *Annu Rev Physiol, 57,* 707-736.

Guo, C., Li, Z., Shi, Y., Xu, M., Wise, J. G., Trommer, W. E. & Yuan, J. (2004). Intein-mediated fusion expression, high efficient refolding, and one-step purification of gelonin toxin. *Protein Expr Purif, 37,* 361-367.

Ikura, M., Clore, G. M., Gronenborn, A. M., Zhu, G., Klee, C. B. & Bax, A. (1992). Solution structure of a calmodulin-target peptide complex by multidimensional NMR. *Science, 256,* 632-638.

Israel, O. K. (2010). Univeristy of Waterloo.

Jurado, L. A., Chockalingam, P. S. & Jarrett, H. W. (1999). Apocalmodulin. *Physiol Rev, 79,* 661-682.

Keller, R. (2004). *The Computer Aided Resonance Assignment Tutorial,* (Editor ed.). Ζυριχη, Switzerland: CANITINA Verlag.

Klee, C. B., Crouch, T. H. & Richman, P. G. (1980). Calmodulin. *Ann. Rev. Biochem., 49,* 489-515.

Knudsen, G. M., Nishida, C. R., Mooney, S. D. & Ortiz de Montellano, P. R. (2003). Nitric-oxide synthase (NOS) reductase domain models suggest a new control element in endothelial NOS that attenuates calmodulin-dependent activity. *J Biol Chem, 278,* 31814-31824.

Kuboniwa, H., Tjandra, N., Grzesiek, S., Ren, H., Klee, C. B. & Bax, A. (1995). Solution structure of calcium-free calmodulin. *Nat Struct Biol, 2,* 768-776.

Lee, S. J. & Stull, J. T. (1998). Calmodulin-dependent regulation of inducible and neuronal nitric-oxide synthase. *J Biol Chem, 273,* 27430-27437.

Li, H., Raman, C. S., Martasek, P., Masters, B. S. & Poulos, T. L. (2001). Crystallographic studies on endothelial nitric oxide synthase complexed with nitric oxide and mechanism-based inhibitors. *Biochemistry, 40,* 5399-5406.

Loscalzo, J. & Vita, J. A. (2000). *Nitric oxide and the cardiovascular system,* (Editor ed.). Totowa, N.J.: Humana Press.

Matsubara, M., Hayashi, N., Titani, K. & Taniguchi, H. (1997). Circular dichroism and 1H NMR studies on the structures of peptides derived from the calmodulin-binding domains of inducible and endothelial nitric-oxide synthase in solution and in complex with calmodulin. Nascent alpha-helical structures are stabilized by calmodulin both in the presence and absence of Ca2+. *J Biol Chem, 272,* 23050-23056.

Matter, H., Kumar, H. S., Fedorov, R., Frey, A., Kotsonis, P., Hartmann, E., Frohlich, L. G., Reif, A., Pfleiderer, W., Scheurer, P., Ghosh, D. K., Schlichting, I. & Schmidt, H. H. (2005). Structural analysis of isoform-specific inhibitors targeting the tetrahydrobiopterin binding site of human nitric oxide synthases. *J Med Chem, 48***,** 4783-4792.

Montelione, G. T., Zheng, D., Huang, Y. J., Gunsalus, K. C. & Szyperski, T. (2000). Protein NMR spectroscopy in structural genomics. *Nat Struct Biol, 7 Suppl***,** 982-985.

Montgomery, H. J., Romanov, V. & Guillemette, J. G. (2000). Removal of a putative inhibitory element reduces the calcium-dependent calmodulin activation of neuronal nitric-oxide synthase. *J Biol Chem, 275***,** 5052-5058.

New England BioLabs, I. (2006). IMPACT^{TM}-CN Instruction Manual.

Newman, E. (2003). *Chemistry*. Waterloo: University of Waterloo.

O'Neil, K. T. & DeGardo, W. F. (1990). How calmodulin binds its targets: sequence independent recognition of amphiphilic α-helices. *Trends Biochem Sci, 15***,** 6.

Reid, D. G. (1997). *Protein NMR techniques,* (Editor ed.). Totowa, N.J.: Humana Press.

Rhoads, A. R. & Friedberg, F. (1997). Sequence motifs for calmodulin recognition. *FASEB J, 11***,** 331-340.

Roberts, G. C. K. (1993a). *NMR of macromolecules : a practical approach,* (Editor ed.). Oxford ; New York: IRL Press at Oxford University Press.

Roberts, G. C. K. (1993b). *NMR of macromolecules : a practical approach,* (Editor ed.). Oxford ; New York: IRL Press at Oxford University Press.

Roman, L. J., Miller, R. T., de La Garza, M. A., Kim, J. J. & Siler Masters, B. S. (2000). The C terminus of mouse macrophage inducible nitric-oxide synthase attenuates electron flow through the flavin domain. *J Biol Chem, 275***,** 21914-21919.

Rosenfeld, R. J., Garcin, E. D., Panda, K., Andersson, G., Aberg, A., Wallace, A. V., Morris, G. M., Olson, A. J., Stuehr, D. J., Tainer, J. A. & Getzoff, E. D. (2002). Conformational changes in nitric oxide synthases induced by chlorzoxazone and nitroindazoles: crystallographic and computational analyses of inhibitor potency. *Biochemistry, 41***,** 13915-13925.

Roskoski, R. (1996). *Biochemistry,* (Editor ed.). Philadelphia: Saunders.

Salerno, J. C., Harris, D. E., Irizarry, K., Patel, B., Morales, A. J., Smith, S. M., Martasek, P., Roman, L. J., Masters, B. S., Jones, C. L., Weissman, B. A., Lane, P., Liu, Q. & Gross, S. S. (1997). An autoinhibitory control element defines calcium-regulated isoforms of nitric oxide synthase. *J Biol Chem, 272***,** 29769-29777.

Schagger, H. & von Jagow, G. (1987). Tricine-sodium dodecyl sulfate-polyacrylamide gel electrophoresis for the separation of proteins in the range from 1 to 100 kDa. *Anal Biochem, 166***,** 368-379.

Schumacher, M. A., Rivard, A. F., Bachinger, H. P. & Adelman, J. P. (2001). Structure of the gating domain of a Ca2+-activated K+ channel complexed with Ca2+/calmodulin. *Nature, 410***,** 1120-1124.

Sheta, E. A., McMillan, K. & Masters, B. S. (1994). Evidence for a bidomain structure of constitutive cerebellar nitric oxide synthase. *J Biol Chem, 269***,** 15147-15153.

Spratt, D. E. (2008). Calmodulin Binding and Activation of Mammalian Nitric Oxide Synthase. *Chemistry*. (p. 369). Waterloo: University of Waterloo.

Spratt, D. E., Israel, O. K., Taiakina, V. & Guillemette, J. G. (2008). Regulation of mammalian nitric oxide synthases by electrostatic interactions in the linker region of calmodulin. *Biochim Biophys Acta, 1784***,** 2065-2070.

Spratt, D. E., Newman, E., Mosher, J., Ghosh, D. K., Salerno, J. C. & Guillemette, J. G. (2006). Binding and activation of nitric oxide synthase isozymes by calmodulin EF hand pairs. *FEBS J, 273*, 1759-1771.

Spratt, D. E., Taiakina, V. & Guillemette, J. G. (2007a). Calcium-deficient calmodulin binding and activation of neuronal and inducible nitric oxide synthases. *Biochim Biophys Acta, 1774*, 1351-1358.

Spratt, D. E., Taiakina, V., Palmer, M. & Guillemette, J. G. (2007b). Differential binding of calmodulin domains to constitutive and inducible nitric oxide synthase enzymes. *Biochemistry, 46*, 8288-8300.

Stuehr, D. J., Tejero, J. & Haque, M. M. (2009). Structural and mechanistic aspects of flavoproteins: electron transfer through the nitric oxide synthase flavoprotein domain. *FEBS J, 276*, 3959-3974.

Vaillancourt, P. E. (2003). *E. coli gene expression protocols,* (Editor ed.). Totawa, N.J.: Humana Press.

Valentine, K. G., Ng, H. L., Schneeweis, L., Kranz, J. K., Frederick, K. K., Alber, T. & Wand, A. J. (2006). Crystal structure of calmodulin-neuronal nitric oxide synthase complex.

Van Eldik, L. J. & Watterson, D. M. (1998). *Calmodulin and signal transduction,* (Editor ed.). San Diego: Academic Press.

Venema, R. C., Ju, H., Zou, R., Ryan, J. W. & Venema, V. J. (1997). Subunit interactions of endothelial nitric-oxide synthase. Comparisons to the neuronal and inducible nitric-oxide synthase isoforms. *J Biol Chem, 272*, 1276-1282.

Venema, R. C., Sayegh, H. S., Arnal, J. F. & Harrison, D. G. (1995). Role of the enzyme calmodulin-binding domain in membrane association and phospholipid inhibition of endothelial nitric oxide synthase. *J Biol Chem, 270*, 14705-14711.

Venema, R. C., Sayegh, H. S., Kent, J. D. & Harrison, D. G. (1996). Identification, characterization, and comparison of the calmodulin-binding domains of the endothelial and inducible nitric oxide synthases. *J Biol Chem, 271*, 6435-6440.

Wei, C. C., Wang, Z. Q., Tejero, J., Yang, Y. P., Hemann, C., Hille, R. & Stuehr, D. J. (2008). Catalytic reduction of a tetrahydrobiopterin radical within nitric-oxide synthase. *J Biol Chem, 283*, 11734-11742.

Wüthrich, K. (1986). *NMR of proteins and nucleic acids,* (Editor ed.). New York: Wiley.

Xia, C., Misra, I., Iyanagi, T. & Kim, J. J. (2009). Regulation of interdomain interactions by calmodulin in inducible nitric-oxide synthase. *J Biol Chem, 284*, 30708-30717.

Yamniuk, A. P. & Vogel, H. J. (2004). Calmodulin's flexibility allows for promiscuity in its interactions with target proteins and peptides. *Mol Biotechnol, 27*, 33-57.

Yuan, T., Vogel, H. J., Sutherland, C. & Walsh, M. P. (1998). Characterization of the Ca2+ -dependent and -independent interactions between calmodulin and its binding domain of inducible nitric oxide synthase. *FEBS Lett, 431*, 210-214.

Zhang, J., Martasek, P., Paschke, R., Shea, T., Siler Masters, B. S. & Kim, J. J. (2001). Crystal structure of the FAD/NADPH-binding domain of rat neuronal nitric-oxide synthase. Comparisons with NADPH-cytochrome P450 oxidoreductase. *J Biol Chem, 276*, 37506-37513.

Zhang, M., Tanaka, T. & Ikura, M. (1995). Calcium-induced conformational transition revealed by the solution structure of apo calmodulin. *Nat Struct Biol, 2*, 758-767.